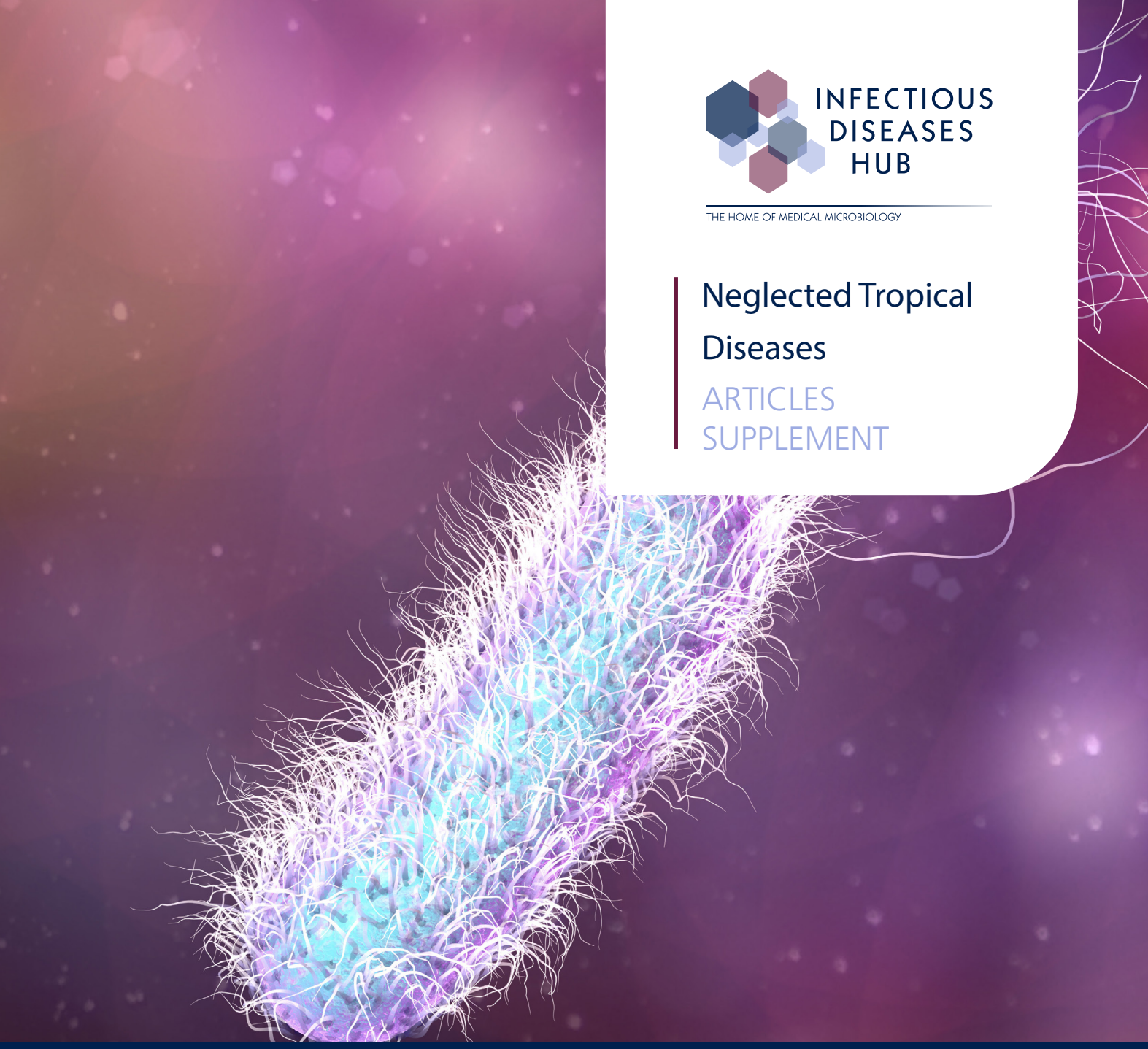

INFECTIOUS DISEASES HUB

THE HOME OF MEDICAL MICROBIOLOGY

Neglected Tropical Diseases

ARTICLES SUPPLEMENT

CONTENTS

fsg CONNECT

Future VIROLOGY

COMMENTARY

How do host restriction factors influence dengue virus replication?



Federico Giovannoni[1], Peter Hemmerich[2] & Cybele Carina García*[,1]

First draft submitted: 13 September 2016; Accepted for publication: 10 October 2016; Published online: 22 November 2016

KEYWORDS
• dengue virus • host factors
• restriction factors

Dengue virus (DENV 1–4) is a major emerging arthropod-borne pathogen, endemic to the tropical and subtropical regions of the world, and infecting 390 million individuals annually. DENV infections can either proceed without symptoms, resulting in self-limited dengue fever, or, as increasingly reported, can develop more severe manifestations in patients, such as dengue hemorrhagic fever and dengue shock syndrome.

Considerable breakthroughs have been made in recent years in the understanding of the structure of DENV particles, life cycle and disease pathogenesis. However, despite the identification of many host and viral factors that either promote or protect the host from severe symptoms of the disease, both the complex nature of their mutual interactions during natural infection, along with the absence of a suitable animal model makes it difficult to fully understand the pathogenesis of severe and fatal cases.

A significant effort is being made by the scientific community to understand the role of each particular molecule within the complex network of interactions existing between host and viral factors. The most common experimental approaches to elucidate the function of a molecule are either to deplete it by blocking the expression of its gene or to alter its activity by introducing loss-of-function mutations. Due to their high efficiency and efficacy and low cost compared with other techniques, high-throughput genome-wide RNAi screening approaches are the most powerful tools for the identification of host factors and pathways involved in any step of a viral replication cycle. Upon depletion of a particular host cell factor, virus multiplication can be either reduced or increased. Thus, according to the loss-of-function phenotype, host factors are classified either as pro- or anti-viral host factors.

Well-established antiviral host factors have been shown to interfere with viral entry, early postentry steps, viral budding and even reduce the infectious quality of extracellular released particles. Most of these have been first identified in the context of the HIV-1 life cycle [1]. However, in the last years these studies have been

"It is very important to understand the functions of factors mediating intrinsic immunity which may lead to the development of new pharmacological agents that can increase its activity and hence lead to treatments..."

[1]Laboratorio de Estrategias Antivirales, Departamento de Química Biológica (QB), Facultad de Ciencias Exactas y Naturales (FCEyN), Universidad de Buenos Aires (UBA) – Instituto de Química Biológica de la Facultad de Ciencias Exactas y Naturales (IQUIBICEN)-Consejo Nacional de Investigaciones Científicas y Técnicas (CONICET), Buenos Aires, Argentina
[2]Leibniz Institute on Aging – Fritz-Lipman-Institut, Jena, Germany
*Author for correspondence: cygarcia@qb.fcen.uba.ar

Future Medicine part of fsg

expanded to other viruses of major public health impact such as influenza, human cytomegalovirus and several flaviviruses, including West Nile, hepatitis C and dengue viruses [2–6].

These antiviral host proteins, often termed as 'host restriction factors', end up inhibiting the replication of viruses, which in return are naturally selected leaving only the most fit to evade and defend themselves against this form of host immunity.

Host restriction factors have certain particularities that differentiate them from other gene products: they act in a dominant and autonomous manner to exert their antiviral activity, they can be either constitutively expressed or upregulated by interferons (IFNs), they can inhibit specific processes in viral replication, they have unusually diverse amino acid sequences as a result of cell–virus co-evolution and they are often antagonized by viral proteins.

In particular, DENV infected cells attempt to restrain virus replication through intrinsic defense mechanisms and the expression of hundreds of IFN-stimulated genes (ISGs) [7]. Several groups have demonstrated that the expression of ISGs, such as viperin, the IFN-induced transmembrane proteins (IFITM2, IFITM3), double-stranded RNA-dependent protein kinase (PKR) and ISG-20 and BST2 inhibit DENV replication [8–10]. Most recently, ISG15 was found to play an anti-DENV function via protein ISGylation. In addition, ISG12b2 was recognized as a novel inner mitochondrial membrane ISG that regulates mitochondria-mediated apoptosis during DENV infection [11,12].

"According to our current results, the disruption of promyelocytic leukemia protein-nuclear bodies during dengue virus 2 infection might be a consequence of the interaction between a viral component and a promyelocytic leukemia protein-nuclear bodies constituent..."

Flaviviruses are considered to be cytoplasmic, since the major part of the viral life cycle (i.e., translation, replication and virion morphogenesis) occurs in the host cell cytoplasm. However, several positive-strand RNA viruses, including the flavivirus DENV, contain genes that code for factors that interact with the host nucleus and/or its components impairing the host cell response and ensuring a successful outcome of viral infection. Strategy can be either to sequester nuclear factors and/or to alter host gene expression by means of virally encoded nuclear proteins counteracting cellular antiviral response. While the precise role of the nucleus in cytoplasmic flaviviruses infection has remained somewhat elusive, evidence now indicates that the viral protein nuclear targeting might have a critical role in the regulation of viral replication/assembly and in subversion of host immunity. Interestingly, extracellular DENV production can be reduced by inhibiting cytoplasmic-nuclear traffic [13].

The genome of DENV is a positive-sense single-stranded approximately 11-kb-sized RNA consisting of an open reading frame from which a polypeptide of roughly 3400 amino acids is generated. The polyprotein is edited proteolytically via viral and host proteases into three structural proteins, capsid (C), pre-membrane (prM) and envelope (E), and seven nonstructural (NS) proteins: NS1, NS2A, NS2B, NS3, NS4A, NS4B and NS5.

So far, three DENV components are considered as interesting candidates for this virus cell nuclear interaction: C, NS5 and NS3. The C protein of many flaviviruses localizes to the nuclei of several infected cell lines (as early as 6 h after infection); the underlying basis and function of which still remains poorly understood and open to debate. Nucleolar accumulation of the C protein may result from its interaction with certain nucleolar proteins or RNAs, whose diverse functions include ribosome synthesis, mRNA processing and DNA replication, as well as cell cycle regulation and stress responses. The C protein might modulate the functions of these nucleolar protein complexes so as to maintain the infected cells at a stage that allows optimal virus replication. Also, the C protein might help to control certain cellular stress responses to the infection, including apoptosis, to minimize premature cell dysfunction and death [14]. NS5 is the largest and most conserved protein encoded by the DENV genome. Recently, different mechanistic studies indicate that binding of NS5 to the spliceosome reduces the efficiency of pre-mRNA processing, independently of NS5 enzymatic activities, and it was proposed that NS5 binding to U5 snRNP proteins hijacks the splicing machinery resulting in a less restrictive environment for viral replication [15].

In addition, this protein is involved in viral RNA synthesis and counteracts the IFN defense system. NS5 localizes on membrane-associated replicase complexes in the cytoplasm and the nucleus of infected cells and was shown to shuttle between the nucleus and the cytoplasm [16]. Last, NS3 is also a flavivirus protein that has been observed to have a nuclear localization.

We have recently demonstrated that one mediator of the intrinsic antiviral defense against DENV is the promyelocytic leukemia protein (PML). PML is a nuclear regulatory protein that is constitutively expressed, but in addition the PML promoter contains elements that trigger

its upregulation in response to the activation of the antiviral IFN pathway. It has been observed that PML interacts with itself and other proteins, especially those that have been modified by small ubiquitin-like modifier (SUMO) proteins, allowing PML to serve as the nucleating constituent of the so-called PML nuclear bodies (PML-NBs) [17]. PML plays a role in numerous cellular pathways and in most cases PML responds to stress conditions to slow or limit growth. Thus, PML could certainly be a host factor that interacts with C, NS5 and NS3 viral proteins. However, the mechanism of the cellular antiviral activity against DENV is not yet understood.

Initial evidence that PML-NBs might be involved in the infection signaling/pathway network is based on the observation of PML body disassembly during DENV-2 infection [18]. According to our current results, the disruption of PML-NBs during DENV-2 infection might be a consequence of the interaction between a viral component and a PML-NB constituent, as part of the viral counter activity against antiviral cellular defense. The alteration of PML-NBs might also be due to a competition for SUMOylation between the DENV proteins suspected of interacting with a protein of the SUMOylation system [19,20], and PML, which is extensively post-translationally modified by SUMOylation, acetylation, ubiquitination and phosphorylation. These post-translational modifications are essential for the activity of PML, and its ability to form NBs and respond to cellular signals. Thus, DENV proteins might be competing with PML for this post-translational modification.

Altogether, these studies should provide a better understanding of the cellular antiviral activity against DENV infection. It is very important to understand the functions of factors mediating intrinsic immunity which may lead to the development of new pharmacological agents that can increase its activity and hence lead to treatments for this viral disease. Also, these studies should shed light upon the functional consequences of DENV proteins nuclear localization and how these processes could be part of DENV strategy to successfully infect and replicate in the cell.

Financial & competing interests disclosure

Research was supported by grants from Agencia Nacional de Promoción Científica y Tecnológica PICT 517, Consejo Nacional de Investigaciones Científicas y Técnicas (CONICET) and Universidad de Buenos Aires (UBA), Argentina. The funders had no role in study design, data collection and analysis, decision to publish, or preparation of the manuscript. CC García is member of Research Career from CONICET. F Giovannoni is a fellow from CONICET and EMBO. The authors have no other relevant affiliations or financial involvement with any organization or entity with a financial interest in or financial conflict with the subject matter or materials discussed in the manuscript apart from those disclosed.

No writing assistance was utilized in the production of this manuscript.

References

1 Bieniasz PD. Restriction factors: a defense against retroviral infection. *Trends Microbiol.* 11(6), 286–291 (2003).

2 Wang X, Hinson ER, Cresswell P. The interferon-inducible protein viperin inhibits influenza virus release by perturbing lipid rafts. *Cell Host Microbe* 2, 96–105 (2007).

3 Seo JY, Yaneva R, Hinson ER, Cresswell P. Human cytomegalovirus directly induces the antiviral protein viperin to enhance infectivity. *Science* 332, 1093–1097 (2011).

4 Lazear HM, Diamond MS. New insights into innate immune restriction of west nile virus infection. *Curr. Opin. Virol.* 11, 1–6 (2015).

5 Zhou LY, Zhang LL. Host restriction factors for hepatitis C virus. *World J. Gastroenterol.* 22(4), 1477–1486 (2016).

6 Pan XB, Han JC, Cong X, Wei L. BST2/tetherin inhibits dengue virus release from human hepatoma cells. *PLoS ONE* 7(12), e51033 (2012).

7 Stetson DB, Medzhitov R. Type 1 interferons in host defense. *Immunity* 25(3), 373–381 (2006).

8 Fink J, Gu F, Ling L *et al.* Host gene expression profiling of dengue virus infection in cell lines and patients. *PLoS Negl. Trop. Dis.* 1(2), e86 (2007).

9 Jiang D, Weidner JM, Qing M *et al.* Identification of five interferon-induced cellular proteins that inhibit West Nile virus and dengue virus infections. *J. Virol.* 84, 8332–8341 (2010).

10 Brass AL, Huang IC, Benita Y *et al.* The IFITM proteins mediate cellular resistance to influenza A H1N1 virus, West Nile virus, and dengue virus. *Cell* 139, 1243–1254 (2009).

11 Lu MY, Liao F. Interferon-stimulated gene ISG12b2 is localized to the inner mitochondrial membrane and mediates virus-induced cell death. *Cell Death Differ.* 18, 925–936 (2011).

12 Dai J, Pan W, Wang P. ISG15 facilitates cellular antiviral response to dengue and West Nile virus infection *in vitro*. *Virol. J.* 8, 468 (2011).

13 Tay MY, Fraser JE, Chan WK *et al.* Nuclear localization of dengue virus (DENV) 1–4 non-structural protein 5; protection against all 4 DENV serotypes by the inhibitor ivermectin. *Antiviral Res.* 99(3), 301–306 (2013).

14 Sangiambut S, Keelapang P, Aaskov J *et al.* Multiple regions in dengue virus capsid protein contribute to nuclear localization during virus infection. *J. Gen. Virol.* 89, 1254–1264 (2008).

15 De Maio FA, Risso G, Iglesias NG *et al.* The dengue virus NS5 protein intrudes in the cellular spliceosome and modulates splicing. *PLoS Pathog.* 12(8), e1005841 (2016).

16 Hannemann H, Sung PY, Chiu HC *et al.* Serotype-specific differences in dengue virus

non-structural protein 5 nuclear localization. *J. Biol. Chem.* 288, 22621–22635 (2013).

17 Van Damme E, Laukens K, Dang TH, Van Ostade X. A manually curated network of the PML nuclear body interactome reveals an important role for PML-NBs in SUMOylation dynamics. *Int. J. Biol. Sci.* 6, 51–67 (2010).

18 Giovannoni F, Damonte EB, García CC. Cellular promyelocytic leukemia protein is an important dengue virus restriction factor. *PLoS ONE* 10(5), e0125690 (2015).

19 Chiu MW, Shih HM, Yang TH, Yang YL. The type 2 dengue virus envelope protein interacts with small ubiquitin-like modifier-1 (SUMO-1) conjugating enzyme 9 (Ubc9). *J. Biomed. Sci.* 14(3), 429–444 (2007).

20 Su CI, Tseng CH, Yu CY, Lai MM. SUMO modification stabilizes dengue virus nonstructural protein 5 to support virus replication. *J. Virol.* 90(9), 4308–4319 (2016).

SPECIAL REPORT

For reprint orders, please contact: reprints@futuremedicine.com

Future VIROLOGY

RNAi agents as chikungunya virus therapeutics

Deepti Parashar*[,1] & Sarah Cherian[1]

Chikungunya virus (CHIKV) is a mosquito-borne emerging pathogen that presents a major health impact in humans. The virus causes acute febrile illness accompanied by joint pains and, in many cases, persistent arthralgia lasting for weeks to years. There are currently no licensed antiviral agents available against CHIKV. A few lead compounds and natural products have recently shown promising results and could emerge as effective treatments for CHIKV. Further, with the emerging knowledge of the biology of CHIKV, RNAi-based gene silencing approaches also hold great promise for the treatment of CHIKV. This review summarizes the applicability of RNAi agents, siRNA, shRNA and miRNA central to RNAi as therapeutic approaches against CHIKV.

First draft submitted: 15 January 2016; Accepted for publication: 3 March 2016;
Published online: 15 April 2016

KEYWORDS
• chikungunya • miRNA
• RNAi • shRNA • siRNA

Chikungunya virus (CHIKV) is a mosquito-transmitted alphavirus belonging to the family *Togaviridae*. The re-emergence of CHIKV in many parts of the world after a gap of nearly 32 years with the 2005–2006 CHIKV fever epidemic in the Indian Ocean island of La Reunion [1] is of a significant public health concern. Subsequently, the virus is reported to have infected millions of individuals in >40 countries, including Malaysia, India, Thailand, Indonesia, Singapore, the USA and some European countries [2,3].

CHIKV is responsible for an acute infection, characterized by high fever, arthralgia, myalgia, headache and rash. Like other alphaviruses, the CHIKV is an enveloped virus with a genome approximately 11.8 kb in size. It consists of a linear, positive sense ssRNA, which is capped and polyadenylated, and encodes two open reading frames (ORFs) **(Figure 1)**. The 5′ ORF encodes four nonstructural proteins (nsP1–nsP4), while the 3′ ORF encodes the structural proteins (the capsid C, envelope glycoproteins E1 and E2, and two small cleavage products: E3, 6K). The nonstructural proteins of CHIKV have vital roles involving enzymatic activities and specific interactions with both viral and host components during different stages of viral pathogenesis, including modulation of cellular antiviral responses [4]. Primarily, nsP1 is involved in viral mRNA capping, nsP2 acts as a protease and helicase, nsP3 functions as an accessory protein involved in RNA synthesis, and nsP4 functions as the RNA-dependent RNA polymerase. An untranslated junction region (J) of 65 nt was observed between the two ORFs. Therefore, the 5′ and 3′ proximal sequences of the RNA genome also carry nontranslatable regions (NTR).

Similar to other alphaviruses, CHIKV starts its life cycle by entering the target host cells via a pH-dependent endocytosis and through a receptor-mediated interaction [5]. Although not fully

[1]National Institute of Virology, 20-A, Dr Ambedkar Road, Pune 411001, Maharashtra, India
*Author for correspondence: deeptiparasharster@gmail.com

Future Medicine part of fsg

understood, PHB [6], HSP70 [7], phosphatidylserine (PtdSer)-mediated virus entry-enhancing receptors (PVEERs) [8], glycosaminoglycans (GAGs) [9], ITGAV and ITGB1 dimer have been suggested as CHIKV receptor proteins [10]. The atomic structure of the complete E3–E2–E1 glycoprotein complex of the CHIKV obtained using X-ray crystallography, provides a structural basis for explaining many biological properties of the virus [11]. E2 is largely responsible for interactions with the cellular receptors while E1 mediates virus host cell membrane fusion, releasing the nucleocapsid into the cytoplasm [12]. The nonstructural proteins precursors (P1234 and P123) are translated from the viral mRNA and further cleaved successively by the nsP2 protease to produce fully mature nsPs and switching the RNA template for synthesis of positive sense genomic RNAs **(Figure 1)** [13]. Promoters present in the negative-stranded RNA intermediate, regulated by nsP4 and the p123 precursor, initiate the transcription of 26S subgenomic positive-stranded RNA, which encodes the structural proteins precursors. The E2 precursor, p62, forms heterodimers in the endoplasmic reticulum with E1 that further transits to the plasma membrane and interacts with nucleocapsids to initiate budding of icosahedral virions [14]. Morphologically, CHIKV replication complexes, as with other alphaviruses, are seen as 65–70 nm spherical invaginations of the membrane, also called spherules.

The replication of CHIKV has been shown to occur in various cell types, such as epithelial, endothelial, fibroblasts and monocyte-derived macrophages [5]. Subsequent to intradermal inoculation by infected mosquitoes, CHIKV replication starts immediately as it enters the subcutaneous capillaries of the skin. Furthermore, the virus disseminates quite rapidly into the circulatory system, thus having access to various parts of the body, including the liver, muscle, joints and brain [15].

Thus far, due to the lack of licensed vaccines or effective antivirals against CHIKV, most of the treatment regimens are symptomatic and based on the clinical manifestations. Nonsalicylate analgesics and NSAIDs are most commonly used for symptomatic relief [16]. Immune-based control strategies have also been tested and have shown effectiveness to some extent [17–19]. Some of the commonly used NSAIDs (methotrexate) and nonsalicylate analgesics have played a major role in symptomatic treatment of the

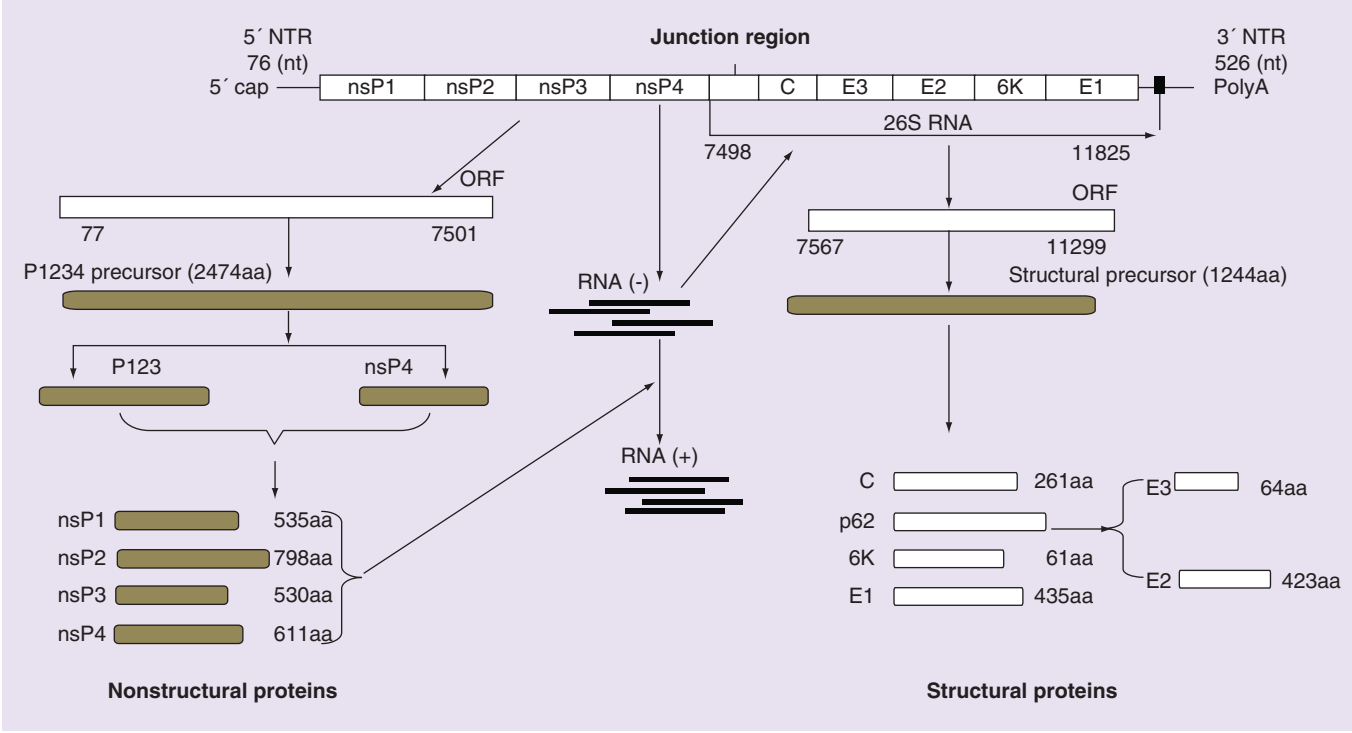

Figure 1. Organization of the chikungunya virus genome and gene products.
NTR: Nontranslatable region; ORF: Open reading frame.

chikungunya disease [20,21]. In addition, some compounds that have been tested against the CHIKV infection include chloroquine [22], ribavirin [23], 6-azauridine [24], arbidol [25] and harringtonine [26]. Among these, few novel lead compounds and natural products were found to have shown promising results as reported in recent reviews [27,28].

RNAi is the process of sequence-specific, post-transcriptional gene silencing in a variety of species, for example, plants, fungi and animals. RNAi regulates gene expression in mammalian cells, as well as acts as a cellular defense mechanism against invaders, including viruses. RNAi, an accurate and potent gene silencing method, was first experimentally documented in *Caenorhabditis elegans* in 1998 [29]. It has been widely employed to manipulate gene expression, elucidate signal pathways and identify gene function at a whole-genome scale.

There are three RNA agents in the RNAi pathway: siRNAs, shRNA and miRNAs that are generated via processing of longer dsRNA and stem-loop precursors [30–32]. During RNAi, long transcripts of dsRNA are rapidly processed into siRNAs, which represent RNA duplexes of specific length and structure that finally guide sequence-specific degradation of mRNAs homologous in sequence to the siRNAs. Converse to siRNAs, the miRNAs and shRNAs are derived from the processing of endogenously encoded stem-loop precursor RNAs. These approximately 22-nt RNAs [33,34], can play important regulatory roles in animals and plants by targeting mRNAs for cleavage or translational repression. miRNAs, shRNAs and siRNAs have shared central biogenesis and can perform interchangeable biochemical functions. Thus, the three classes of silencing RNAs cannot be distinguished by either their chemical composition or mechanism of action. RNAi approaches have been attempted against viral infections including influenza [35], hepatitis B [36,37] and hepatitis C [38], dengue [39], HIV [40], etc. Here we will present the mechanism of RNAi in brief, discuss the three RNAi agents: siRNAs, shRNA and miRNAs in the context of CHIKV inhibition and summarize RNAi as a therapeutic approach against CHIKV.

Mechanisms of RNAi

The RNAi response is activated when the exogenous dsRNA incorporated into the cytoplasm of the viral cell is recognized by RNase type III, Dicer, resulting in the formation of a siRNA. Synthetically engineered siRNAs can also be administered directly to the cytoplasm through a suitable delivery system. The siRNA is bound to a protein complex called RNA-induced silencing complex (RISC), where a helicase unwinds the duplex siRNA. The resulting antisense strand guides the RISC to its complementary target mRNA, which will be cleaved, thereby preventing translation [34,41–42].

On the other hand, a shRNA is created endogenously in the cell nucleus using a plasmid or viral vector. shRNAs can be transcribed through either RNA polymerase II or III. The first transcript generates a hairpin like stem–loop structure that is processed by a complex containing the RNase type II enzyme, Drosha. The individual pre-shRNAs generated are finally transported to the cytoplasm by exportin-5 where they are cleaved by the cellular machinery into siRNA. miRNA is transcribed from DNA as primary miRNA, which is frequently synthesized from intronic regions of protein-coding RNA polymerase II transcripts [43,44]. The primary miRNA is processed into dsRNAs or precursor miRNA, a hairpin intermediate of 70 nt [45], by two proteins: Drosha and Pasha. Precursor miRNA are then transported to the cytoplasm, and after cleavage and processing by Dicer to yield RNA duplexes and unwinding to obtain the miRNA, the subsequent steps are identical to those that occur with siRNA and shRNA as illustrated in **Figure 2**.

Among the diverse RNAi-based mechanisms, miRNAs are highly conserved in mammals and hence it is believed that miRNA-based silencing may contribute to the post-transcriptional regulation of at least a third of the mammalian mRNAs [46].

The miRNA-like mechanism is further believed to be faster than the siRNA-like mechanism, since the latter acts via perfect complementarity for a target message [47]. It has been demonstrated that both miRNAs and siRNAs can suppress translation of mRNAs (in the case of an imperfect match) and can cleave targeted RNAs (in the case of a perfect match). It has also been observed that shRNA can act via miRNA- or siRNA-like mechanism [48].

RNAi agents (siRNA, shRNA & miRNA) against CHIKV

RNAi offers a promising approach toward inhibiting viral protein expression through selectively

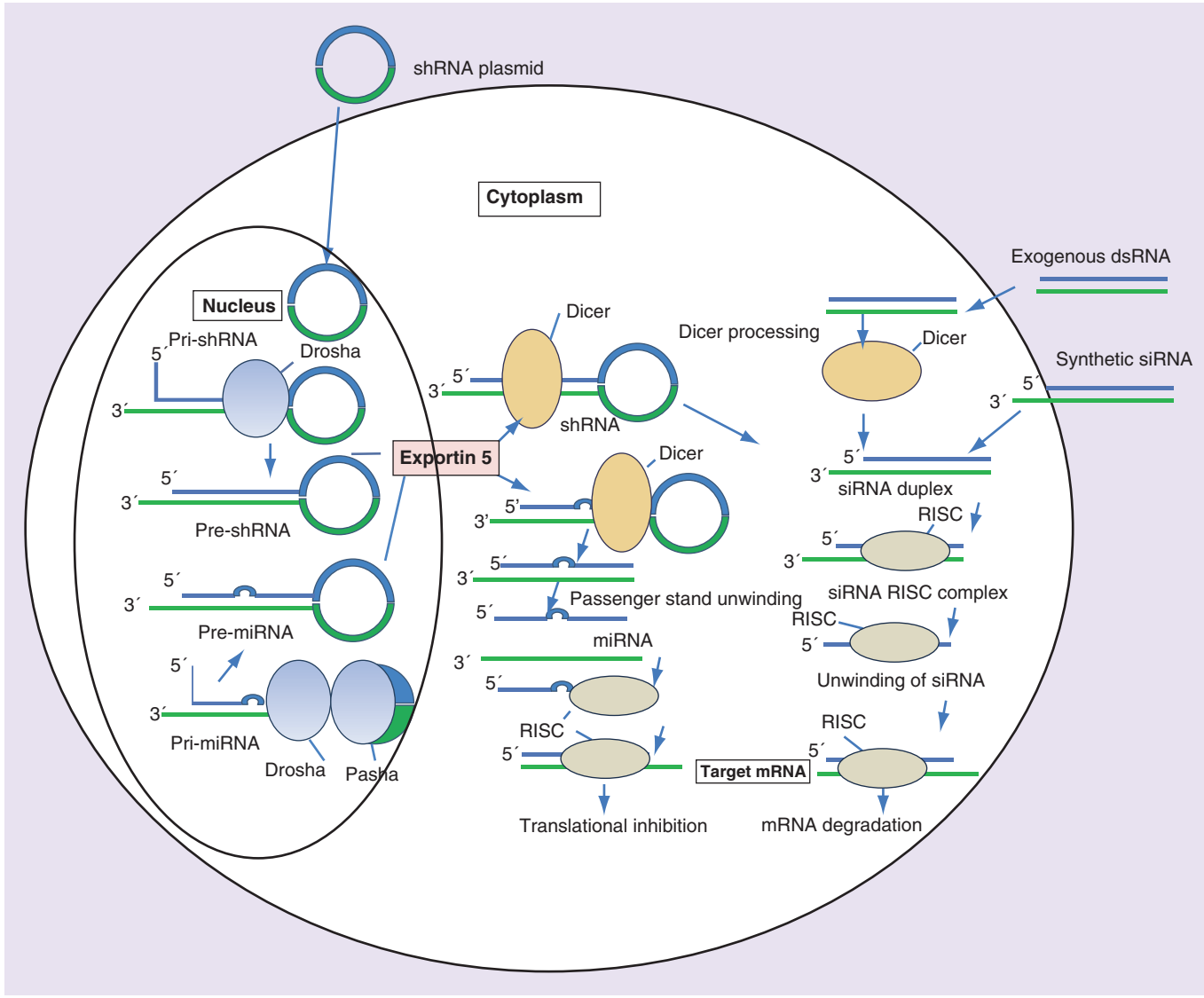

Figure 2. RNAi mechanism: differences between siRNA, shRNA and miRNA as therapeutic tools.
RISC: RNA-induced silencing complex.

targeting the viral genome template. Like most RNA viruses, translation of the CHIKV genome is carried out by the host-cell translation machinery.

The CHIKV RNA can be predicted to be highly susceptible to RNAi agents as replication occurs in the cytoplasm, its genome resembles eukaryotic mRNAs and thus most regions of CHIKV RNA are accessible to RNAi machinery that would lead to a decrease in protein expression and decline in genomic RNA.

• siRNA

The therapeutic application of siRNA against *nsP3* and *E1* genes for the inhibition of CHIKV replication has been examined in Vero cells **(Figure 3)** [49]. The results indicated a reduction of virus titer up to 99.6% in siRNA-transfected cells compared to control. The viral inhibition was most significant at 24 h (99%). However, the success of this study is limited as siRNAs used were demonstrated to reduce replication by 65% by 48 h postinfection and not evaluated *in vivo*.

Another study conducted by our group designed eight siRNAs targeting the *E2* or the *nsP1* genes of CHIKV **(Figure 3)**. Results showed two of the siRNAs efficiently inhibited CHIKV replication in virus-infected Vero-E6 cells and mice. CHIKV replication was completely inhibited in virus-infected mice when administered 72 h postinfection. A combination of the two siRNAs

exhibited additive effect leading to early and potent inhibition of virus replication. Our findings suggested the promising efficacy of RNAi in silencing sequence-specific genes of CHIKV that can constitute a new therapeutic strategy for controlling the CHIKV infection and transmission [28,50].

• shRNA

The efficacy of plasmid-based shRNA against CHIKV replication in three CHIKV-permissive cell lines, namely, HeLa, human muscle rhabdomyosarcoma RD cells and Baby Hamster Kidney BHK-21 cells has been investigated [51]. The study demonstrated that a plasmid-based shRNA expression system directed against CHIKV *E1* and *nsP1* genes was effective in producing sustained inhibition against CHIKV replication in stable shRNA-expressing cell clones. Both shRNA E1 and nsP1 cell clones showed complete suppression of CHIKV E2 protein expression while shRNA against the capsid demonstrated a modest inhibitory effect as compared to scrambled shRNA cell clones and nontransfected cell controls. On the other hand, a noninhibitory trend of shRNA E1 was observed against dengue and Sindbis virus, indicating the high specificity of the shRNA against CHIKV replication. Thus, even after 50 passages of CHIKV in the stable cell clones, no shRNA-resistant CHIKV mutant was generated. Evaluation of the efficacy of the antiviral activity of the shRNA in C57BL/6 mice demonstrated strong and sustained anti-CHIKV protection in suckling mice pretreated with different concentrations (3.1, 9.5 and 19 pmol) of shRNA E1. Survival of the pretreated mice was observed up to day 15 postinfection as compared with the manifestation of CHIKV symptoms and CHIKV-induced lethality in nontreated and scrambled shRNA-treated mice. Overall, the data provide strong evidence of the anti-CHIKV efficacy of shRNA *in vivo* and reinforces the potential usefulness of shRNA in clinical settings of CHIKV infection [51].

• miRNA

Research on miRNAs is providing vast opportunities for developing therapeutic approaches to treatment of infectious diseases, and especially viral infections [52]. Recent animal and even human efficacy data have shown that oligonucleotides to target miRNAs known as anti-miR compounds have the prospective to become an entirely new class of drugs [53].

In a study by Saxena *et al.* [54], microarray technology and quantitative PCR method was used to establish the complete miRNA signature of host response upon CHIKV infection in a human cell line infection model, human embryonic kidney cell line (HEK293T). The results of miRNA expression profiling revealed regulation of a total of 152 miRNAs of which 65 were up and 33 were down, 12 hr post-CHIKV infection. Among the top upregulated miRNAs, the induction of miR-744, miR-638 and miR-503 was noted. The miRNA signature established in this study could point toward potential miRNA targets, which may be used for therapeutic purpose.

In another study, the role of miR-146a in modulation of inflammatory responses of human synovial fibroblasts by CHIKV was studied. It was shown that CHIKV induces expression levels of miR-146a in primary human synovial fibroblasts. This in turn suppresses TRAF6, IRAK1, IRAK2 expression levels and downstream NF-κB activity through a negative feedback loop. CHIKV utilizes miR-146a, as a negative regulator of general antiviral response [55].

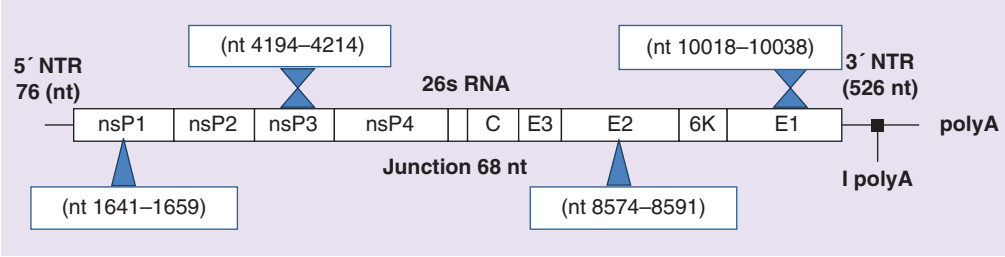

Figure 3. Sites of the siRNA target sequences within the chikungunya virus genome. Dark-filled dumbbells represent the locations of the siRNAs target sequences as implemented by Dash *et al.* [49], and triangles represent locations of target sequences implemented by Parashar *et al.* [50]. The numbers in bracket denote the start and end nucleotide position in the chikungunya virus genomic sequence.
NTR: Nontranslatable region.

Shrinet *et al.* [56] have identified and analyzed the distribution and abundance of known and novel miRNAs in *Aedes albopictus*, and evaluated their modulation upon CHIKV infection. Their investigations provide an insight about cellular modification by miRNAs during CHIKV infection and the results provide leads for identifying potential candidates for vector-based antiviral strategies.

Recent studies in our laboratory have helped identify the analogous miRNA expression profile following CHIKV infection and target genes in mice and human skin fibroblast cells. Results are suggestive that the putative target genes of the differentially expressed miRNAs are involved in RIG-I pathway, TGF-β signaling pathway, JAK-STAT signaling pathway, MAPK signaling pathway, cytokine–cytokine receptor interactions and Fcγ R-mediated phagocytosis. The results further indicate the potential use of miR15, miR-16, miR-17, let-7e, miR-125, miR-99 and miR-23a as biomarkers of CHIKV infection. MiRNAs, such as miR-15a, miR-16, miR-140, miR-146a, miR-155, miR203, miR223, miR-499 and miR-363, known to be implicated in rheumatoid arthritis [57–63], notably showed differential regulation in CHIKV infection. Given that the mouse has been used as a model organism for CHIKV biomedical research and antiviral screening, miRNA expression profiles of mice can potentially serve as useful biomarkers in understanding the CHIKV biology [Parashar *et al.*, Unpublished Data].

Advantages & limitations of RNAi therapeutics

When compared with other therapies, RNAi-based antiviral strategies have a number of advantages. Unlike small molecule inhibitors, the design of siRNAs is straight forward and simple, due to the availability of number algorithms implementing rules for their design [64,65]. Moreover, with the existence of genome sequence libraries, highly specific siRNAs can be designed, with reduced potential for off-targeting or undesired effects [66,67], enabling specificity of the gene silencing and thus increased siRNA efficacy [68]. Furthermore, compared with small molecule inhibitors, the synthesis of siRNAs is also relatively easy.

In comparison to other antisense strategies, for example, antisense DNA oligonucleotides and ribozymes, RNAi is much more potent [69]. Single-stranded small antisense RNAs may also be loaded into RISC and guide target mRNA cleavage, although with a much reduced efficiency [70]. The high potency of RNAi implies that the effector molecules may function at much lower concentrations, which is an important factor for therapeutics.

Moreover, as siRNA is able to affect multiple steps in the viral life cycle, it is able to reduce the levels of viral transcripts and proteins even in the absence of active viral replication, such as in the liver cell of chronically infected patients. The gene silencing effect of siRNA is a short transitional effect usually lasting for 3–7 days before naturally disappearing [71]. This lowers the chance of side effects as observed with other therapeutic methods, such as IFN-α and ribavirin.

Furthermore, the cytoplasmic location of the RNAi machinery, such as Dicer, RISC, etc., makes the RNAi approach technically easier than other methods in which the silencer needs to be taken up by the nucleus to exert an effect [72]. RNAi-based therapies also do not cause any toxicity that can result from introducing a foreign compound into the body as they mimic a natural process and effect existing protein complexes [73].

Despite these advantages, a major issue regarding the use of RNAi-based therapies against virus infections, particularly RNA viruses, is the emergence of escape mutants during the process of viral replication and evolution [74]. Appropriate choice of the target site and use of a pool of siRNAs to simultaneously target multiple sites in the viral genome may help overcome this concern to some extent [75].

Theoretically, the siRNA is able to specifically block the synthesis of any protein responsible for any disease; however, the actual translation of siRNA into clinical use has been hampered by several difficulties. These include the need to protect siRNA from degradation by nucleases in biological fluids, the delivery of siRNA to target tissues and the intracellular delivery of siRNA to the cytoplasm of target cells where RNAi takes place. The efficient delivery of RNAi effectors is one of the greatest hurdles for clinical translation. Direct administration of dsRNA in the form of siRNAs complexed to lipids has been shown to activate innate inflammatory pathways [76]. The use of recombinant adeno-associated vectors provides the potential of lifelong persistence of RNAi, and also the ability to achieve systemic delivery, though the combined toxicity imparted by the viral vector itself, is of concern [77]. However, preclinical and clinical trials with recombinant adeno-associated vectors are extensive and showing promising results [77].

Conclusion & future perspective

Chikungunya illness in humans is often characterized by abrupt onset of fever, headache, fatigue, nausea, vomiting, rash, myalgia and severe arthralgia. Painful polyarthralgia is a common symptom and persists in a small proportion of cases for several months. However, there currently is no licensed vaccine or therapeutic measure available to combat chikungunya infection. Understanding the fundamental biology of RNAi has led to its widespread application in basic research and subsequently in applications for the treatment of disease. It is expected in the coming years that we will understand more about RNAi-mediated regulation of gene expression and, thus, see RNAi-based drugs approved for use in disease therapy. RNAi has also proven to be a powerful tool for the study of gene function and has revealed new avenues for basic investigation. siRNAs form attractive drug candidates because of their potency, selectivity and versatility. The development of siRNA therapies, however, has been hampered by the difficulty in their delivery to the target cell type, tissue or organ, as they do not readily cross the cellular membrane owing to their negative charge and size. Several groups have studied the use of viral vectors to introduce shRNAs into organisms, although the safety of viral vectors for therapeutic use is still questioned. Recent improvements in lipid chemistries, chemical modifications and advances in eliminating specific motifs have reduced, but not eliminated, the potential serious side effects of lipid-based delivery systems. Issues concerning the cellular delivery of siRNA agents and their stability, etc., are further being addressed via a range of delivery vectors (e.g., polymers, liposomes and nanoparticles).

These nonviral delivery vectors address the safety risk and manufacturing cost though they are less effective than viral vectors. Nanoparticles have also been recognized as a principal delivery vehicle for gene therapy. Nanotechnology holds great promise for medicines for various reasons, for example, multiple selectivity, desirable solubility and permeability, a favorable pharmacokinetic profile, tunable tissue specificity, higher stability under physiological conditions and the ability to scale-up during manufacture.

In spite of the disadvantages, several RNAi-based therapies have been used in clinical trials, and are in the process of evaluation in standard pharmacokinetic and Phase I safety studies. Hopefully, in the near future, the siRNA approach may provide a better and effective treatment that will lead to the control and management of the chikungunya infection.

Financial & competing interests disclosure

The siRNA sequences (Parashar et al.*, 2013) discussed in the text have been filed for Indian patent (application no. 1960/DEL/2013) and PCT (application no. PCT/IN2014/000441). The authors have no other relevant affiliations or financial involvement with any organization or entity with a financial interest in or financial conflict with the subject matter or materials discussed in the manuscript apart from those disclosed.*

No writing assistance was utilized in the production of this manuscript.

EXECUTIVE SUMMARY

RNAi agents as chikungunya virus therapeutics

- RNAi is a sequence-specific, post-transcriptional gene-silencing mechanism of most eukaryotic cells that uses small dsRNA molecules.
- Three basic RNAi strategies: siRNA, shRNA and miRNA have been applied as therapeutics against the chikungunya virus, an alphavirus that has emerged as a major public health problem in several countries recently.

Advantages of RNAi-based approaches

- A major advantage of RNAi versus other antisense-based approaches for therapeutic applications is that it utilizes cellular machinery that allows efficient targeting of complementary transcripts, often resulting in highly potent target gene silencing.

Conclusion & future perspective

- Though the results are promising, the agents need to be evaluated for pharmacokinetic, as well as safety studies in clinical trials.
- Cellular delivery of these macromolecules also needs to be fully addressed.

References

Papers of special note have been highlighted as:
• of interest; •• of considerable interest

1 Schuffenecker I, Iteman I, Michault A *et al.* Genome microevolution of chikungunya viruses causing the Indian Ocean outbreak. *PLoS Med.* 3, 1058–1070 (2006).

2 Arankalle VA, Shrivastava S, Cherian S *et al.* Genetic divergence of chikungunya viruses in India (1963–2006) with special reference to the 2005–2006 explosive epidemic *J. Gen. Virol.* 88, 1967–1976 (2007).

3 Cherian SS, Walimbe AM, Jadhav SM *et al.* Evolutionary rates and timescale comparison of chikungunya viruses inferred from the whole genome/*E1* gene with special reference to the 2005–07 outbreak in the Indian subcontinent. *Infect. Gen. Evol.* 9, 16–23 (2009).

4 Fros JJ, Liu WJ, Prow NA *et al.* Chikungunya virus nonstructural protein 2 inhibits type I/II interferon-stimulated JAK-STAT signaling. *J. Virol.* 84, 10877–10887 (2010).

5 Sourisseau M, Schilte C, Casartelli N *et al.* Characterization of reemerging chikungunya virus. *PLoS Pathog.* 3, e89 (2007).

6 Wintachai P, Wikan N, Kuadkitkan A *et al.* Identification of prohibitin as a chikungunya virus receptor protein. *J. Med. Virol.* 84, 1757–1770 (2012).

7 Paingankar MS, Arankalle VA. Identification of chikungunya virus interacting proteins in mammalian cells. *J. Biosci.* 39, 389–399 (2014).

8 Moller-Tank S, Kondratowicz AS, Davey RA, Rennert PD, Maury W. Role of the phosphatidylserine receptor TIM-1 in enveloped-virus entry. *J. Virol.* 87, 8327–8341 (2013).

9 Silva LA, Khomandiak S, Ashbrook AW *et al.* A single-amino-acid polymorphism in chikungunya virus E2 glycoprotein influences glycosaminoglycan utilization. *J. Virol.* 88, 2385–2397 (2014).

10 Takada Y, Ye X, Simon S. The integrins. *Genome Biol.* 8, e215 (2007).

11 Voss JE, Vaney MC, Duquerroy S *et al.* Glycoprotein organization of chikungunya virus particles revealed by X-ray crystallography. *Nature* 468, 709–712 (2010).

12 Kielian M. Class II virus membrane fusion proteins. *Virology* 344, 38–47 (2006).

13 Shirako Y, Strauss JH. Regulation of Sindbis virus RNA replication: uncleaved P123 and nsP4 function in minus-strand RNA synthesis, whereas cleaved products from P123 are required for efficient plus-strand RNA synthesis. *J. Virol.* 68, 1874–1885 (1994).

14 Pletnev SV, Zhang W, Mukhopadhyay S *et al.* Locations of carbohydrate sites on alphavirus glycoproteins show that E1 forms an icosahedral scaffold. *Cell* 105, 127–136 (2001).

15 Caglioti C, Lalle E, Castilletti C, Carletti F, Capobianchi MR, Bordi L. Chikungunya virus infection: an overview. *New Microbiol.* 36, 211–227 (2013).

16 Pialoux G, Gauzere BA, Jaureguiberry S, Strobel M. Chikungunya, an epidemic arbovirosis. *Lancet Infect. Dis.* 7, 319–327 (2007).

17 Ozden S, Lucas-Hourani M, Ceccaldi PE *et al.* Inhibition of chikungunya virus infection in cultured human muscle cells by furin inhibitors: impairment of the maturation of the E2 surface glycoprotein. *J. Biol. Chem.* 283, 21899–21908 (2008).

18 Brehin AC, Casademont I, Frenkiel MP, Julier C, Sakuntabhai A, Despres P. The large form of human 2′,5′- oligoadenylate synthetase (OAS3) exerts antiviral effect against chikungunya virus. *Virology* 384, 216–222 (2009).

19 Khan M, Dhanwani R, Patro IK, Rao PVL, Parida MM. Cellular IMPDH enzyme activity is a potential target for the inhibition of chikungunya virus replication and virus induced apoptosis in cultured mammalian cells. *Antiviral Res.* 89, 1–8 (2011).

20 Suhrbier A, Linn ML. Clinical and pathologic aspects of arthritis due to Ross River virus and other alphaviruses. *Curr. Opin. Rheumatol.* 16, 374–379 (2004).

21 Hoarau JJ, Bandjee MCJ, Trotot PK *et al.* Persistent chronic inflammation and infection by chikungunya arthritogenic alphavirus in spite of a robust host immune response. *J. Immunol.* 184, 5914–5927 (2010).

22 Delogu I, de Lamballerie X. Chikungunya disease and chloroquine treatment. *J. Med. Virol.* 83, 1058–1059 (2011).

23 Ravichandran R, Manian M. Ribavirin therapy for chikungunya arthritis. *J. Infect. Dev. Ctries* 2, 140–142 (2008).

24 Briolant S, Garin D, Scaramozzino N, Jouan A, Crance JM. *In vitro* inhibition of chikungunya and Semliki Forest viruses replication by antiviral compounds: synergistic effect of interferon-alpha and ribavirin combination. *Antiviral Res.* 61, 111–117 (2004).

25 Delogu I, Pastorino B, Baronti C, Nougairede A, Bonnet E, de Lamballerie X. *In vitro* antiviral activity of arbidol against chikungunya virus and characteristics of a selected resistant mutant. *Antiviral Res.* 90, 99–107 (2011).

26 Kaur P, Thiruchelvan M, Lee RCH *et al.* Inhibition of chikungunya virus replication by harringtonine, a novel antiviral that suppresses viral protein expression *Antimicrob. Agents Chemother.* 57, 155–167 (2013).

27 Rashad A, Mahalingam S, Keller PA. Chikungunya virus: emerging targets and new opportunities for medical chemistry. *J. Med. Chem.* 57, 1147–1166 (2014).

28 Parashar D, Cherian S. Antiviral perspectives for chikungunya virus. *Biomed. Res. Int.* 2014, 631642 (2014).

• **A systematic review on antiviral perspectives for chikungunya virus including inhibitors based on RNA-mediated interference.**

29 Fire A, Xu S, Montgomery MK, Kostas SA, Driver SE, Mello CC. Potent and specific genetic interference by double-stranded RNA in *Caenorhabditis elegans*. *Nature* 391, 806–811 (1998).

•• **Describes how dsRNA was substantially more effective at producing interference than either strand individually.**

30 Novina CD, Murray MF, Dykxhoorn DM *et al.* siRNA-directed inhibition of HIV-1 infection. *Nat. Med.* 8, 681–686 (2002).

31 Yin JQ, Wan Y. siRNA-mediated gene regulation system. *Int. J. Mol. Med.* 10, 355–365 (2002).

32 Tijsterman M, Plasterk, . Dicers at RISC; the mechanism of RNAi. *Cell* 117(1), 1–3 (2004).

33 Hannon GJ, Rossi JJ. Unlocking the potential of the human genome with RNA interference. *Nature* 431(7006), 371–378 (2004).

34 Meister G, Tuschl T. Mechanisms of gene silencing by double stranded RNA. *Nature* 431, 343–349 (2004).

•• **Describes the mechanisms of gene silencing by dsRNA.**

35 Khanna M, Saxena L, Rajput R, Kumar B, Prasad R. Gene silencing: a therapeutic approach to combat influenza virus infections. *Future Microbiol.* 10, 131–140 (2015).

36 Maepa MB, Roelofse I, Ely A, Arbuthnot P. Progress and prospects of anti-HBV gene therapy development. *Int. J. Mol. Sci.* 16, 17589–17610 (2015).

37 Gish RG, Yuen MF, Chan HL *et al.* Synthetic RNAi triggers and their use in chronic hepatitis B therapies with curative intent. *Antiviral Res.* 121, 97–108 (2015).

38 Motavaf M, Safari S, Alavian SM. Therapeutic potential of RNA interference: a new molecular approach to antiviral treatment for hepatitis C. *J. Viral Hepat.* 19, 757–765 (2012).

39 Idrees S, Ashfaq UA. RNAi: antiviral therapy against dengue virus. *Asian Pac. J. Trop. Biomed.* 3, 232–236 (2013).

40 Jacque JM, Triques K, Stevenson M. Modulation of HIV-1 replication by RNA interference. *Nature* 418, 435–438 (2002).

41 Hammond SM. Dicing and slicing: the core machinery of the RNA interference pathway. *FEBS Lett.* 579, 5822–5829 (2005).

42 Liu J, Carmell MA, Rivas FV *et al.* Argonaute2 is the catalytic engine of mammalian RNAi. *Science* 305, 1437–1441 (2004).

43 Cai X, Hagedorn CH, Cullen BR. Human microRNAs are processed from capped, polyadenylated transcripts that can also function as mRNAs. *RNA* 10, 1957–1966 (2004).

44 Lee Y, Kim M, Han J *et al.* MicroRNA genes are transcribed by RNA polymerase II. *EMBO J.* 23, 4051–4060 (2004).

45 Lee Y, Ahn C, Han J *et al.* The nuclear RNase III Drosha initiates microRNA processing. *Nature* 425, 415–419 (2003).

46 Meunier J, Lemoine F, Soumillon M *et al.* Birth and expression evolution of mammalian microRNA genes. *Genome Res.* 23, 34–45 (2013).

47 Rao DD, Vorhies JS, Senzer N, Nemunaitis J. siRNA versus shRNA: similarities and differences. *Adv. Drug Deliv. Rev.* 61, 746–759 (2009).

48 Taft RJ, Pang KC, Mercer TR, Dinger M, Mattick JS. Non-coding RNAs: regulators of disease. *J. Pathol.* 220, 126–139 (2010).

49 Dash PK, Tiwari M, Santhosh SR, Parida M, Lakshmana Rao PV. RNA interference mediated inhibition of chikungunya virus replication in mammalian cells. *Biochem. Biophys. Res. Commun.* 376, 718–722 (2008).

• **First report of the effectiveness of siRNA against *in vitro* replication of chikungunya virus.**

50 Parashar D, Paingankar MS, Kumar S *et al.* Administration of E2 and NS1 siRNAs inhibit chikungunya virus replication *in vitro* and protects mice infected with the virus. *PLoS Neg. Trop. Dis.* 7, e2405 (2013).

•• **First *in vivo* experiment that revealed siRNA therapy is effective *in vivo* by reducing the clinical symptoms in the challenge-infected animals and was capable of reducing virus replication in serum and muscles.**

51 Lam S, Chen KC, Ng MM *et al.* Expression of plasmid based shRNA against the *E1* and *nsP1* genes effectively silenced chikungunya virus replication. *PLoS ONE* 7, e46396 (2012).

• **Describes the efficacy of plasmid-based shRNA against chikungunya virus replication.**

52 Cullen BR. Viruses and RNA interference: issues and controversies. *J. Virol.* 88, 12934–12936 (2014).

53 van Rooij E, Purcell AL, Levin AA. Developing microRNA therapeutics. *Circ.Res.* 110, 496–507 (2012).

54 Saxena T, Tandon B, Sharma S *et al.* Combined miRNA and mRNA signature identifies key molecular players and pathways involved in chikungunya virus infection in human cells. *PLoS ONE* 8, e79886 (2013).

55 Selvamani SP, Mishra R, Singh SK. Chikungunya virus exploits mir-146a to regulate NF-κB pathway in human synovial fibroblasts. *PLoS ONE* 9, e103624 (2014).

56 Shrinet J, Jain S, Jain J, Bhatnagar RK, Sunilm S. Next generation sequencing reveals regulation of distinct aedes microRNAs during chikungunya virus development. *PLoS Negl. Trop. Dis.* 8, e2616 (2014).

57 Miyaki S, Nakasa T, Otsuki S *et al.* MicroRNA-140 is expressed in differentiated human articular chondrocytes and modulates interleukin-1 responses. *Arthritis Rheum.* 60, 2723–2730 (2009).

58 Nagata Y, Nakasa T, Mochizuki Y *et al.* Induction of apoptosis in the synovium of mice with autoantibody-mediated arthritis by the intra articular injection of double-stranded microRNA-15a. *Arthritis Rheum.* 60, 2677–2683 (2009).

59 Kurowska-Stolarska M, Alivernini S, Ballantine LE *et al.* MicroRNA-155 as a proinflammatory regulator in clinical and experimental arthritis. *Proc. Natl Acad. Sci. USA* 108, 11193–11198 (2011).

60 Stanczyk J, Ospelt C, Karouzakis E *et al.* Altered expression of microRNA-203 in rheumatoid arthritis synovial fibroblasts and its role in fibroblast activation. *Arthritis Rheum.* 63, 373–381 (2011).

61 Chatzikyriakidou A, Voulgari PV, Georgiou I, Drosos AA. miRNAs and related polymorphisms in rheumatoid arthritis susceptibility. *Autoimmun. Rev.* 11, 636–641 (2012).

62 Yang B, Chen J, Li Y *et al.* Association of polymorphisms in pre-miRNA with inflammatory biomarkers in rheumatoid arthritis in the Chinese Han population. *Hum. Immunol.* 73, 101–106 (2012).

63 Shibuya H, Nakasa T, Adachi N *et al.* Overexpression of microRNA-223 in rheumatoid arthritis synovium controls osteoclast differentiation. *Mod. Rheumatol.* 23, 674–685 (2013).

64 Elbashir SM, Lendeckel W, Tuschl T. RNA interference is mediated by 21 and 22 nt RNAs. *Genes Dev.* 15, 188–200 (2001).

65 Naito Y, Ui-Tei K. siRNA design software for a target gene-specific RNA interference. *Front. Genet.* 3, 102 (2012).

66 Semizarov D, Frost L, Sarthy A, Kroeger P, Halbert DN, Fesik SW. Specificity of short interfering RNA determined through gene expression signatures. *Proc. Natl Acad. Sci. USA* 100, 6347–6352 (2003).

67 Jackson AL, Bartz SR, Schelter J *et al.* Expression profiling reveals off-target gene regulation by RNAi. *Nat. Biotechnol.* 21, 635–637 (2003).

68 Chi JT, Chang HY, Wang NN, Chang DS, Dunphy N, Brown PO. Genome wide view of gene silencing by small interfering RNAs. *Proc. Natl Acad. Sci. USA* 100, 6343–6346 (2003).

69 Bertrand JR, Pottier M, Vekris A, Opolon P, Maksimenko A, Malvy C. Comparison of antisense oligonucleotides and siRNAs in cell culture and *in vivo*. *Biochem. Biophys. Res. Commun.* 296, 1000–1004 (2002).

70 Martinez J, Patkaniowska A, Urlaub H, Luhrmann R, Tuschl T. Single-stranded antisense siRNAs guide target RNA cleavage in RNAi. *Cell* 110, 563–574 (2002).

71 Saito Y, Dzik S. Gene knockdown: RNA-interference is coming of age. *Transfusion* 45, 111–114 (2005).

72 Ashfaq UA, Yousaf MZ, Aslam M, Ejaz R, Jahan S, Ullah O. siRNAs: potential therapeutic agents against hepatitis C virus. *Virol. J.* 8, 276 (2011).

73 Manoharan M. RNA interference and chemically modified siRNAs. *Nucleic Acids Res.* 3, 115–116 (2003).

74 Wilson JA, Richardson CD. Hepatitis C virus replicons escape RNA interference induced by a short interfering RNA directed against the NS5b coding region. *J. Virol.* 79, 7050–7058 (2005).

75 Aagaard L, Rossi JJ. RNAi therapeutics: principles, prospects and challenges. *Adv. Drug Deliv. Rev.* 59, 75–86 (2007).

76 Judge AD, Sood V, Shaw JR, Fang D, McClintock K, MacLachlan I. Sequence-dependent stimulation of the mammalian innate immune response by synthetic siRNA. *Nat. Biotechnol.* 23, 457–462 (2005).

77 Borel F, Kay MA, Mueller C. Recombinant AAV as a platform for translating the therapeutic potential of RNA interference. *Mol. Ther.* 22, 692–701 (2014).

Research Article

For reprint orders, please contact: reprints@futuremedicine.com

Nanomedicine

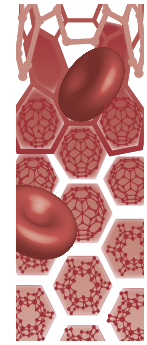

Development of mannose-anchored thiolated amphotericin B nanocarriers for treatment of visceral leishmaniasis

Aim: Our goal was to improve treatment outcomes for visceral leishmaniasis by designing nanocarriers that improve drug biodistribution and half-life. Thus, long-acting mannose-anchored thiolated chitosan amphotericin B nanocarrier complexes (MTC AmB) were developed and characterized. **Materials & methods:** A mannose-anchored thiolated chitosan nanocarrier was manufactured and characterized. MTC AmB was examined for cytotoxicity, biocompatibility, uptake and antimicrobial activities. **Results:** MTC AmB was rod shaped with a size of 362 nm. MTC AmB elicited 90% macrophage viability and 71-fold enhancement in drug uptake compared with native drug. The antileishmanial IC_{50} for MTC AmB was 0.02 μg/ml compared with 0.26 μg/ml for native drug. **Conclusion:** These studies show that MTC can serve as a platform for clearance of *Leishmania* in macrophages.

First draft submitted: 2 September 2016; Accepted for publication: 26 October 2016; Published online: 23 November 2016

Keywords: amphotericin B • macrophage nanoparticle targeting • mannose receptors • thiolated chitosan • visceral leishmaniasis

Gul Shahnaz[1,2], Benson J Edagwa*[,2], JoEllyn McMillan[2], Sohail Akhtar[3], Abida Raza[4], Naveeda A Qureshi[5], Masoom Yasinzai[6] & Howard E Gendelman[2]

[1]Department of Pharmacy, Quaid-i-Azam University Islamabad, 45320, Pakistan
[2]Department of Pharmacology & Experimental Neuroscience, University of Nebraska Medical Center, Omaha, NE 68198, USA
[3]Department of Entomology, University College of Agriculture & Environmental Sciences, The Islamia University, Bahawalpur, Pakistan
[4]Nuclear Medicine, Oncology & Radiotherapy Institute, Islamabad, Pakistan
[5]Department of Animal Sciences, Quaid-i-Azam University, Islamabad, 45320, Pakistan
[6]Centre for Interdisciplinary Research in Basic Sciences, International Islamic University, Islamabad, Pakistan
*Author for correspondence: benson.edagwa@unmc.edu

Visceral leishmaniasis (VL; kala-azar) remains a common tropical infectious disease. *Leishmania* amastigotes and promastigotes target mononuclear phagocytes (MP; monocytes and tissue macrophages), and parasite growth is sustained by the cell's microenvironment. Infection remains high in prevalence, morbidity and mortality in the developing world [1]. The obligate intracellular *Leishmania donovani* amastigotes replicate within membrane-bound MP subcellular organelles. Current medical management is not effective for eliciting microbial clearance due to drug resistance, toxicity, bioavailability and cost [2]. Chemotherapy for VL is based on the use of antimony. However, the emergence of resistance has transformed medical management to the use of amphotericin B (AmB) for VL treatment [2,3]. Notably, targeted intracellular delivery of AmB has now emerged as a first-line medical strategy to facilitate pathogen clearance. The development of improved drug delivery formulations that include nanotechnology-based targeted therapeutics that target infected cells and tissues could improve treatment outcomes [3,4].

It is well accepted that mannose-based carriers can be harnessed to improve antileishmanial drug delivery. This idea is based on the target macrophage surface receptor distribution [2–4]. Proof of concept for such an approach includes, but is not limited to, drugs such as muramyl dipeptide, efavirenz and rifampin [5–7]. Each has yielded encouraging results. Mannose receptors recognize corresponding sugars and facilitate cellular uptake of drug-encased particles [8,9]. Consequent internalization of the therapeutic carrier facilitates drug accumulation at sites of active parasitic infection [8]. Such receptor-mediated MP drug nanoparticle targeting is linked to the effectiveness of the ligand-anchored therapeutic carrier. This serves to improve drug cell entry, retention and cargo

Future Medicine part of fsg

release in an infected or bystander cell [9]. However, the question of finding the optimal vehicle for drug-based macrophage carriages has not yet been addressed. One answer is chitosan-based nanocarriers. These carriers have gained considerable interest due to their tunable functional groups, biocompatibility and biodegradability [10]. Thiolated chitosan (TC) such as chitosan–thioglycolic acid conjugates can be generated by immobilization of thiol groups on the chitosan polymer backbone [11]. Formation of inter- and intramolecular disulfide bonds within the thiolated polymer matrix results in improved properties, such as *in situ* gelling/cohesion that facilitates the drug delivery system stability [12,13]. Specifically, mannosylation of TC polymer (MTC) is believed to be an appealing strategy for targeted intracellular MP delivery of AmB as it would not only aid in parasite clearance but also help reduce the dosing volume and frequency. To date, there is only limited research that has been conducted to investigate the potential of mannose-anchored thiolated nanocarriers for VL and linked parasitic disease therapy [2,3,14]. In this study, improved mannose-anchored TC (MTC) nanocarriers were developed to facilitate stability, biocompatibility, controlled release and cell uptake by macrophages for antileishmanial therapy.

Materials & methods

Materials

Low MW chitosan, cysteine, hydrogen peroxide, Ellman's reagent (5,5-dithiobis[2-nitrobenzoic acid]), AmB, acetonitrile, methanol, mannose and DMSO were purchased from Sigma-Aldrich (MO, USA). Pooled human serum was obtained from Innovative Biologics (VA, USA). Solvents used were HPLC-grade materials.

TC polymer synthesis

The synthesis of the thiolated polymer was made through covalent linkage of thioglycolic acid (TGA) to chitosan by amide bond formation between the polymer amino groups and carboxylate groups of the sulfhydryl moiety [12]. Briefly, chitosan 1% (w/v) was hydrated with 1% (v/v) acetic acid solution. This was by followed the addition of 500 mg of TGA after which 1-ethyl-3-(3-dimethylaminopropyl) carbodiimide hydrochloride-coupling reagent at a final concentration of 100 mM was added to activate the carboxylic acid moieties of TGA. The pH of the reaction mixture was adjusted to 5.5 with 10 M NaOH, and mixtures were incubated for 3.5 h under continuous stirring. The solution was dialyzed five-times in a membrane tubing (MW cut-off 12–14 kDa) for 3 days under protection from light at 10°C in order to separate unbound sulfhydryl moieties from the thiolated polymer. Briefly, the crude thiolated polymer was dialyzed once against 5 mM HCl (5 l), then twice against the same media of 1% (w/v) NaCl to break ionic interactions between the positively charged polymer and the negatively charged sulfhydryl moieties. Finally, the samples were dialyzed thoroughly twice against 1 mM HCl to adjust the pH of the TC solution. The dialyzed product was lyophilized and stored at 4°C for subsequent use.

MTC synthesis & characterization

Mannose was linked onto TC as described with modifications [15]. Mannose immobilization was carried out by reductive amination of TC. Two percent TC was dissolved in 1% v/v aqueous acetic acid by stirring at room temperature. Sodium 0.12 M cyanoborohydride and 0.33 M D-mannose were then added to the resulting viscous polymer solution with vigorous stirring. The resulting reaction mixture was continuously stirred until a white foamy gel was formed. The gel was smashed up then rinsed four-times with 150 ml methanol and once with diethyl ether (150 ml). The light pink solid product was then dried for several hours.

Quantitation of primary amine functional groups at each level of modification was determined by a colorimetric 2,4,6-trinitrobenzenesulfonic acid (TNBS) assay. In this assay, the polymer (0.5 mg) was dissolved in 500 µl NaCl (0.5%, w/v) solution. After incubation at 25°C for 30 min, 500 µl of TNBS (0.1%, w/v) comprising $NaHCO_3$ (4%, w/v) was incorporated into each hydrated aliquot. After 3 h of incubation at 37°C and centrifugation (33,527 × *g*; 5 min; 4°C), absorbance was recorded at 410 nm on a microtiter plate reader (Molecular Devices, CA, USA). L-cysteine HCl standards were used for the calculations.

The degree of conjugation as assessed by the amount of thiol groups anchored to TC and MTC was determined by Ellman's reagent. First, conjugates (0.5 mg) were hydrated in 500 µl of phosphate buffer (0.5 M; pH 8.0). Then 500 µl of Ellman's reagent (3 mg in 10 ml of 0.5 M phosphate buffer) was added into each aliquot. The mixtures were incubated for 3 h at room temperature. The thiol content on TC and MTC was then determined by measuring the absorbance of 300 µl of the mixture at 410 nm on a microtiter plate reader (Molecular Devices). L-cysteine HCl was used as a standard to quantify the sulfhydryl on the MTC.

The extent of disulfide bond formation due to air oxidation during polymer modifications was measured as previously reported [12]. TC and MTC (0.5 mg) were swelled in Falcon tubes (15 ml) containing 1 ml of 0.05 M Tris buffer, pH 6.8. After 30 min of incubation at room temperature, 1 ml of a 4% (w/v) sodium-borohydride solution was added to the reaction mixtures. The

Table 1. Composition (polymer, surfactant, drug and cross-linking agent ratio) and physicochemical characterization including polydispersity index, particle size, payload and ζ-potential of the ionically cross-linked nanocarriers used in study (designated as 1, 2 and 3).

Formulations	Polymer % (m/v)	Tween % (v/v)	TPP (μM)	Drug % (m/v)	Size (nm)	PDI	Payload %	ζ-potential (mv)
Unmodified chitosan								
UC -1	0.3	16.6	0.35	0.1	1048 ± 54	0.83 ± 0.72	21.0	33 ± 2
UC -2	0.3	16.6	0.40	0.1	827 ± 12	0.65 ± 0.31	35.0	30 ± 7
UC -3	0.3	16.6	0.54	0.1	449 ± 38	0.31 ± 0.01	47.0	28 ± 3
Thiolated chitosan								
TC -1	0.3	16.6	0.4	0.1	654 ± 41	0.71 ± 0.06	24.5	29 ± 2
TC -2	0.3	16.6	0.6	0.1	495 ± 13	0.29 ± 0.03	64.8	23 ± 0.9
TC -3	0.3	16.6	0.7	0.1	1032 ± 14	0.61 ± 0.02	35.0	21 ± 4
Mannose-anchored thiolated chitosan								
MTC -1	0.3	16.6	0.4	0.1	1012 ± 18	0.42 ± 0.01	53.8	29 ± 4
MTC -2	0.3	16.6	0.6	0.1	478 ± 9	0.25 ± 0.01	72.9	20 ± 1
MTC -3	0.3	16.6	0.7	0.1	951 ± 27	0.91 ± 0.08	26.0	19 ± 0.8

Indicated values are mean ± SD of at least three experiments.
MTC: Mannose-anchored thiolated chitosan; PDI: Polydispersity index; SD: Standard deviation; TC: Thiolated chitosan; UC: Unmodified chitosan; TPP: Sodium tripolyphosphate.

samples were then oscillated for 3 h in a shaking water bath at 37°C. The mixture was quenched by the addition of 200 μl of 5 M HCl. Ellman's reagent (500 μl of 0.4% [w/v]) was added to determine the remaining thiol content as described above.

Fourier transform IR & proton NMR spectroscopy

Immobilization of mannose on TC was elucidated further by Fourier transform IR (FTIR; Schimadzu, Model 8400, Japan) and proton NMR (^{1}H NMR; 500 MHz; Varian Medical Systems, Inc., CA, USA) spectroscopy. FTIR spectroscopy was acquired by the KBr disk method over the range of 4000–400 cm^{-1}. ^{1}H NMR spectroscopy was conducted in deuterated DMSO.

Preparation of the nanocarriers

Nanocarriers of unmodified chitosan (UC), TC and MTC were synthesized using *in situ* gellation. Specifically, AmB was dissolved in 2.5% (v/v) aqueous acetic acid solution and Tween 80 to a final concentration shown in Table 1. The polymer (0.33%, w/v) was then added to the mixture and the reaction allowed to proceed for 2 h. Afterward the product was mechanically mixed using high-pressure homogenization. The purified nanocarriers were then stabilized by adding an aqueous solution of sodium tripolyphosphate cross-linker at the final concentrations shown in Table 1. The synthesized particles were categorized as either clear, opalescent or agglomerates based on qualitative visual evaluation. The nanocarriers were then partially oxidized with 0.5% (v/v) H_2O_2 solution after incubation for 1 h under continuous stirring at room temperature. The resultant opalescent product of desired physicochemical parameters was selected for further characterization and investigations as shown in Table 2. To prevent particle aggregation during differential centrifugation (33,527 × *g*; 10 min; 4°C), 5% (w/v) trehalose was added to the nanoformulation before this step. After centrifugation, the supernatant was removed and the pellet washed twice with water before resuspending in 0.1% (v/v) aqueous acetic acid solution (2 ml) and stored at 4°C for subsequent use.

Particle size, surface charge and polydispersity index (PDI) of the nanocarriers were determined by dynamic light scattering using a Malvern Zetasizer Nano Series Nano-ZS (Malvern Instruments, Inc., MA, USA). Encapsulation efficiency of AmB in UC, TC and MTC was determined after centrifugation (14,000 × *g*, 60 min, 4°C) of nanoparticle suspensions to remove unentrapped insoluble drug. The pelleted nanocarriers were dissolved in methanol and ultrasonicated for 10 min to facilitate particle rupture. The drug released into the supernatant after centrifugation (14,000 × *g*, 5 min, 4°C) was quantified by HPLC [16]. Drug encapsulation efficiency was calculated using the formula:

$$EE = \frac{\text{Total amount of drug in formulation} - \text{Unentrapped drug}}{\text{Total amount of drug}} \times 100$$

Table 2. Characterization in terms of thiol groups, disulfide bonds, polydispersity index, particle size, payload and ζ-potential of covalently cross-linked (oxidized) nanocarriers.

Formulations	-SH [μMol/g]	-S-S- [μMol/g]	Size (nm)	PDI	Payload %	ζ-potential (mv)
UC	-	-	449 ± 38†*	0.31 ± 0.01	47.0†**	28 ± 4
TC	1283 ± 96	82 ± 27	495 ± 13	0.29 ± 0.03	64.8	23 ± 0.9
Thiolated chitosan (Ox)	857 ± 45	389 ± 52	390 ± 26§*	0.21 ± 0.02	69.5§*	21 ± 0.6
MTC	1269 ± 101	62 ± 18	478 ± 9	0.25 ± 0.01	72.9	20 ± 1
Mannose-anchored Ox	781 ± 95	454 ± 113	362 ± 27‡**	0.22 ± 0.03	78.3‡***	19 ± 3

Values are mean ± SD of at least three experiments. Statistically significant differences were determined between UC and ox TC†; UC and Ox MTC‡; Ox TC and Ox MTC§.
*p < 0.05; **p < 0.01; ***p < 0.001.
MTC: Mannose-anchored thiolated chitosan; Ox: Oxidized; PDI: Polydispersity index; SD: Standard deviation; TC: Thiolated chitosan; UC: Unmodified chitosan.

Stability of the designed nanocarriers was evaluated under various storage conditions. For stability testing, 100 μl aliquots of the nanocarriers were stored at -20, 4 and 37°C over 4 weeks then analyzed for surface charge, size and PDI. Scanning electron microscopy of the nanocarriers was performed using a Hitachi S4700 Field-Emission Scanning Electron Microscope (Hitachi High Technologies America, Inc., IL, USA).

Nanoparticle drug release

The release profile of AmB from UC, TC and MTC nanocarriers was evaluated at macrophage endosomal and physiological pH, 5.5 and 7.4, respectively. Either sodium acetate buffer or phosphate-buffered saline (PBS), each containing 1% (v/v) Tween 80, was used as the release medium. The release rate of native AmB powder was evaluated as a control. An appropriate volume of each nanocarrier suspension was reconstituted in 10 ml of release media to achieve a final concentration of 10 mg/ml and transferred into dialysis bags (MW cut-off 12–14 kDa). The dialysis bags were then immersed in 100 ml of release media and stirred at 37°C. At predetermined time intervals, an aliquot of the medium was drawn and diluted in methanol. The concentration of drug released was determined by HPLC [16].

Parasites, cells & nanoparticle treatments

The WHO reference strain of *L. donovani* promastigotes (MHOM/IN/80/DD8) was obtained from American Type Culture Collection (ATCC® 50212) and is sensitive to AmB. The resistance in the acquired strain was provoked by incremental increases in AmB concentration enabling the pathogen to grow at 500 μM drug concentration. Resistant and sensitive *L. donovani* clinical isolate parasites (1–2 × 10^6 cells/ml) were grown at 25°C in Medium 199 with Hank's Balanced Salts (Thermo Fisher Scientific, MA, USA), plus 10% (v/v) heat-inactivated fetal bovine serum; American Type Culture Collection cat. no. 30–2020) and 50 mg/l gentamicin, in a 75 cm^2 tissue culture flask (14 ml medium) for >4 days to stationery phase (50–100 × 10^6 cells/ml). Macrophage J774 cells were grown in RPMI-1640 medium (HyClone; GE Healthcare Life Sciences, UT, USA) supplemented with 15% (v/v) heat-inactivated fetal bovine serum and 50 mg/l gentamicin at 37°C. The effects of the nanoformulations on cell viability of J774 cells and primary human monocyte-derived macrophages were evaluated using the 3-(4,5-dimethyl-2-thiazolyl)-2,5-diphenyl-2H-tetrazoliumbromide (MTT) assay with minor modifications [2]. Briefly, non-infected J774 cells were seeded at a density of 1 × 10^6 cells/ml in 96-well plates at a volume of 200 μl culture medium/well and incubated for 24 h at 37°C. Depending on surface chemistry nanoformulations had variant encapsulation/associations of AmB with the polymeric nanocarriers; the drug loading capacities were 80%, 70%, and 47% for MTC, TC, and Chito, respectively. To maintain equivalent concentrations, nanoformulations of MTC, TC and UC were dissolved in 100% DMSO and diluted to reach concentrations of 25, 50 and 75 μg/ml AmB in the culture medium. The maximum concentration of DMSO after dilution was 0.1%. Cells treated with 25, 50 or 75 μg/ml of native AmB or no drug constituted control groups. The cells were incubated for 24, 48 or 72 h at 37°C in a 5% CO_2 incubator after nanocarrier treatment. Following incubation, the supernatant was replaced with culture medium containing MTT (500 μg/ml) and further incubated for 4 h at 37°C. To dissolve formazan crystals, 100 μl of DMSO was added and absorbance was measured at 450 nm using a microplate reader.

J774 cell uptake and retention of nanocarriers, AmBisome® and native drug were evaluated as previously described [17]. Briefly, cells were incubated with nanocarriers at 100 μM drug concentrations, and cellular uptake measured over a 12 h period. Adherent cells were washed three-times with PBS and scraped. Cell pellets were collected by centrifugation at 950 × *g* for 10 min then resuspended in 200 μl of methanol,

sonicated and centrifuged. Triplicate 20-µl samples of methanol extracts were assessed by HPLC [16]. For determination of efflux pump inhibition, J774 cells infected with *L. donovani* were treated with 5 µM verapamil, an adenosine triphosphate-binding cassette (ABC) transporter inhibitor. Verapamil was added to the cells with or without parasites and incubated for 2 h prior to treatment with nanoformulations or AmB. After treatment with verapamil the cells were washed with PBS (pH 7.2) and treated with nanoformulations, AmBisome or AmB then processed for microbial uptake [17]. For cell drug retention studies, J774 cells were incubated with nanoformulations for 24 h and washed three-times with PBS. Fresh medium without nanoformulations was added and the cells were cultured for a further 10 days with half medium changes every other day. On days 2, 4, 8 and 10 following nanoformulation treatment, J774 cells were scraped then processed for drug quantitation by HPLC as described for cell uptake.

Antileishmanial activities

An amastigote model in a macrophage cell line was used to evaluate antileishmanial activity of the developed formulations and AmBisome, as reported previously [18]. Briefly, the J774 cells were resuspended (2.5×10^5 cells/ml) in RPMI-1640 culture medium without serum. The cells were plated onto 8-well Lab-Tek CCR^2 tissue culture slides (NUNC; Thermo Fisher Scientific) at a density of 200×10^3 cells/well and incubated at 37°C for 24 h in a humidified incubator. The cells were then washed twice with serum-free medium and infected with 100 µl metacyclic stage of *L. donovani* at an infection ratio of 10:1 (parasites/macrophages) in 200 µl of whole medium (RPMI 1640 + 10% heat-inactivated fetal calf serum + 50 mg/l gentamicin) and incubated for 12 h. Nonphagocytosed parasites were removed by washing three-times with PBS and the wells were resupplemented with RPMI-1640 complete medium. Stock solutions of native AmB and UC, TC, MTC nanocarriers were prepared in 100% DMSO at 1 mg/ml AmB. AmBisome was reconstituted consistent with the manufacturer's protocol to achieve a 5 mg/ml stock of AmB. Working concentrations were prepared in whole medium (RPMI 1640 + 10% heat-inactivated fetal calf serum + 50 mg/l gentamicin). The cells were treated with AmB formulations (Chito, CT, MCT and AmBisome) at six different drug concentrations (1–0.004 µg/ml AmB) prepared by serial dilution. Untreated infected macrophages were used as positive controls. The drug activities of free UC, TC and MTC nanocarriers were also investigated. Each formulation concentration was tested in quadruplicate. The maximum DMSO concentration of 0.1% was found to have no influence on macrophage/amastigote clearance. After 72 h of incubation (5% CO_2 at 37°C), slides were fixed with 100% methanol for 1 min and stained for 10 min with 10% Giemsa's solution. Giemsa-stained intramacrophage amastigotes slides were visualized under a light microscope (Zeiss, AXIO, NY, USA). Percent inhibition from test formulations and AmB were calculated as cells/100 nucleated nontreated control cells. Data were fitted using the nonlinear dose–response sigmoidal curve, and the IC_{50} values were estimated by using Microsoft xl/fit.

In vivo therapeutic efficacy evaluations of the developed nanoformulations were performed according to a protocol approved by the Institutional Animals Ethical Committee of Quaid-i-Azam University, Islamabad, Pakistan. Thirty-six BALB/c mice (20–25 g) were infected by intracardiac injection of 1×10^8 promastigotes of *L. donovani*. After 4 weeks, infection was confirmed in three randomly selected mice by Giemsa staining of splenic tissue. Native-free drug AmB (group I) and nanoformulated UC (group II), TC (group III), MTC (group IV) and drug-free nanocarrier (group V) were administered orally at 1 mg/kg body weight per day for 7 days; whereas the control group (group VI) received an equal volume of saline. In order to validate the data, a single intravenous dose of AmB was administered at 1 mg/kg body weight/day for 7 consecutive days. Treated groups were sacrificed on day 7 post-treatment and compared with untreated infected control animals. The spleen weight was calculated after autopsy and tissue smears were prepared for microscopic examination by Giemsa staining. The percent suppression of splenic parasite load and parasite burden and the percent inhibition of parasite replication were determined using the following formula:

$$PI = \frac{PP - PT}{PP} \times 100$$

where PI is the percent inhibition, PP is the amount of amastigotes/100 macrophage nuclei pretreatment while PT is the amount of amastigotes/100 macrophage nuclei post-treatment in spleen tissue smears.

Statistical analyses

Data sets were investigated for normal distribution by using the Kolmogorov–Smirnov test. Normally distributed data were analyzed using one-way analysis of variance followed by the Tukey's posthoc test. Kruskal–Wallis tests were followed by Dunn's *post hoc* evaluations for non-normally distributed data. All results were expressed as mean ± standard deviation (SD), with n representing the number of repeats. Two-tailed statistical analyses were considered significant at $p < 0.05$ or highly significant at $p < 0.01$.

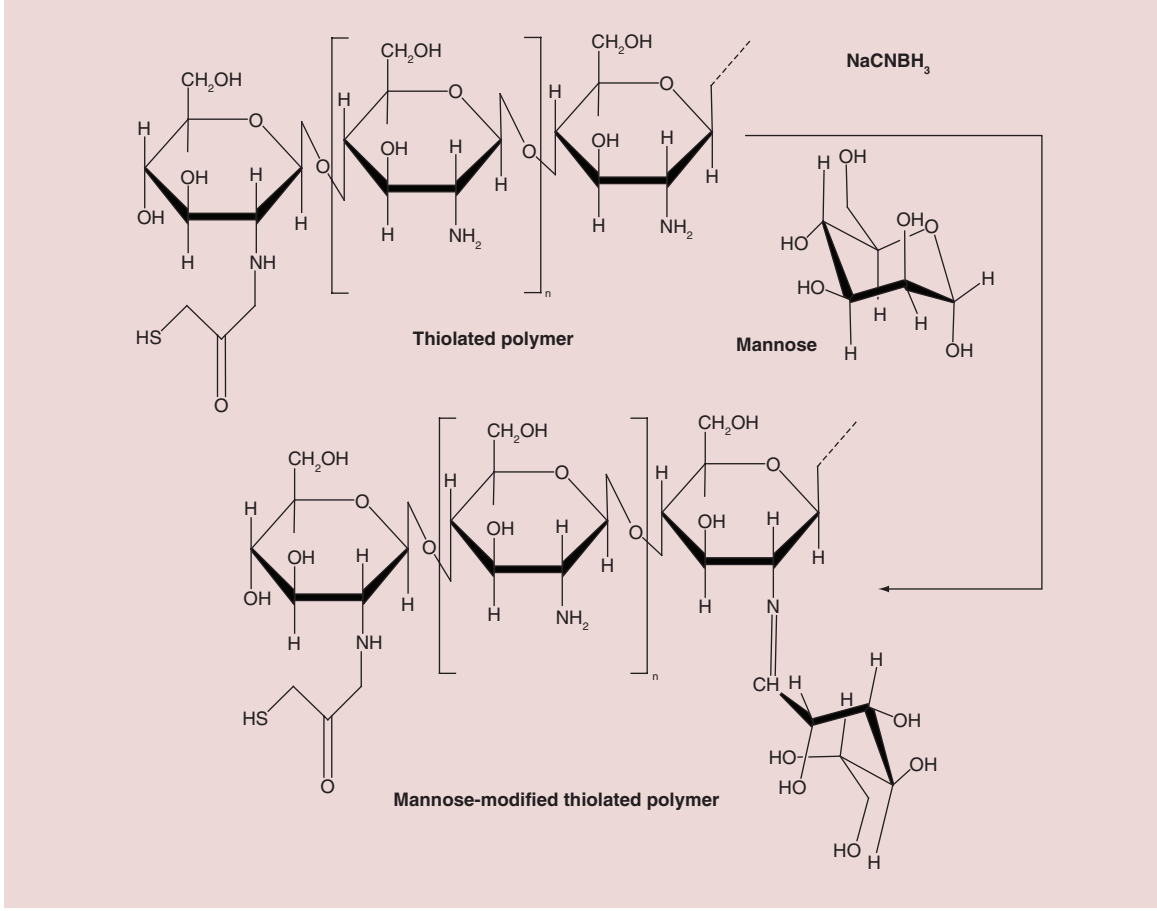

Figure 1. Synthetic scheme for the establishment of mannose-modified chitosan–thioglycolic acid conjugate. The Schiff's base (R-CH = N-R) mediated amide bonds formation between the aldehyde group of mannose and the amino group of the thiolated polymer.

Results

TC synthesis & characterization

Evaluation of the thiol groups immobilized to the thiolated polymer by the Ellman's test demonstrated that on average 1301 ± 194 µmol of thiol groups were attached/gram of polymer (mean ± SD; n = 3). In addition, the amounts of primary amino groups and disulfide bonds within the TC were estimated by TNBS and disulfide bond assays, respectively. According to the data, there were 429 ± 62 µmol primary amino groups per gram of polymer (mean ± SD; n = 3) and 107 ± 12 µmol disulfide bonds/gram of polymer (mean ± SD; n = 3). The reduced disulfide bond formation implied reduced oxidation that had occurred during the conjugation reaction. This demonstrated the high efficiency of the thiolation process. The efficiency of the purification step for the TC polymer was confirmed by comparison to control polymers synthesized similarly but without 1-ethyl-3-(3-dimethylaminopropyl) carbodiimide hydrochloride during the conjugation step. The control polymers exhibited negligible quantities of thiol groups per gram of polymer. The purified polymers were frozen and lyophilized to give white fibrous structures that were readily soluble in aqueous solutions.

MTC nanocarriers

We next sought to determine the utility of thiolated polymer for MP targeting as a therapeutic strategy as a therapy for VL. Mannose modification of the TC polymer was initiated by ring opening of mannose followed by reductive amination reaction of the resultant aldehyde with free amino groups on the TC polymer. The synthetic scheme for this mannose-modified chi-

Figure 2. Characterization of the polymers by nuclear magnetic resonance spectroscopy (see facing page). 1H-NMR spectra comparing unmodified polymer **(A)** and thiolated chitosan **(B)** polymer controls to mannose-anchored thiolated chitosan **(C)**. The presence of methylene peaks (3.5-3.9 ppm and 4.5-5.1 ppm) in the spectrum of the mannose-anchored thiolated chitosan confirmed the attachment of the sugar to the polymer.

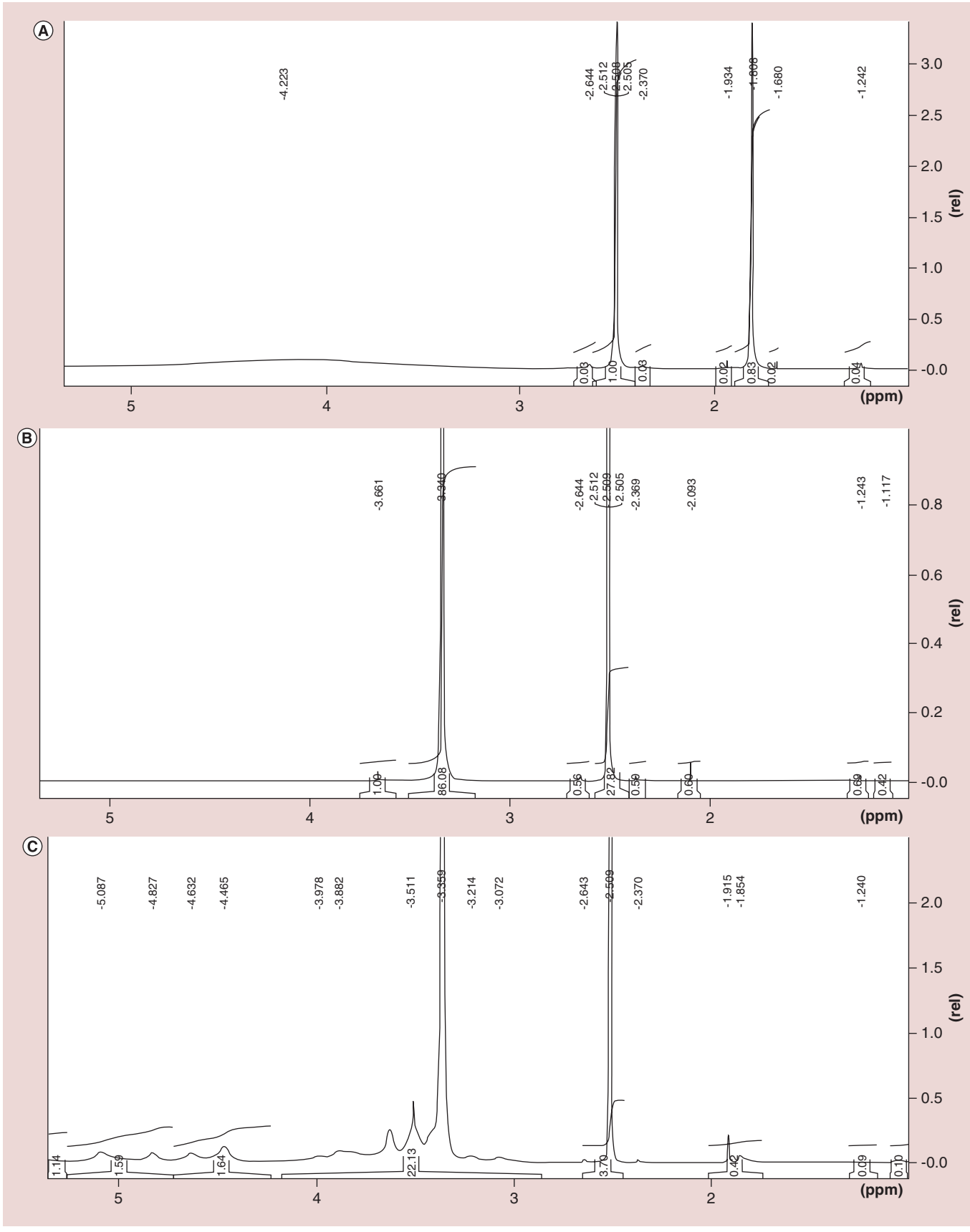
A
-4.223
-2.644
2.512
2.509
2.505
-2.370
-1.934
-1.808
-1.680
-1.242
0.03
1.00
0.08
0.02
0.83
0.02
0.04
(rel)
(ppm)
B
-3.661
-3.340
-2.644
2.512
2.509
2.505
-2.369
-2.093
-1.243
-1.117
1.00
86.08
0.56
27.82
0.59
0.69
0.69
0.42
(rel)
(ppm)
C
-5.087
-4.827
-4.632
-4.465
-3.978
-3.882
-3.511
-3.359
-3.214
-3.072
-2.643
-2.509
-2.370
-1.915
-1.854
-1.240
1.14
1.59
1.64
22.13
3.70
0.42
0.09
0.10
(rel)
(ppm)

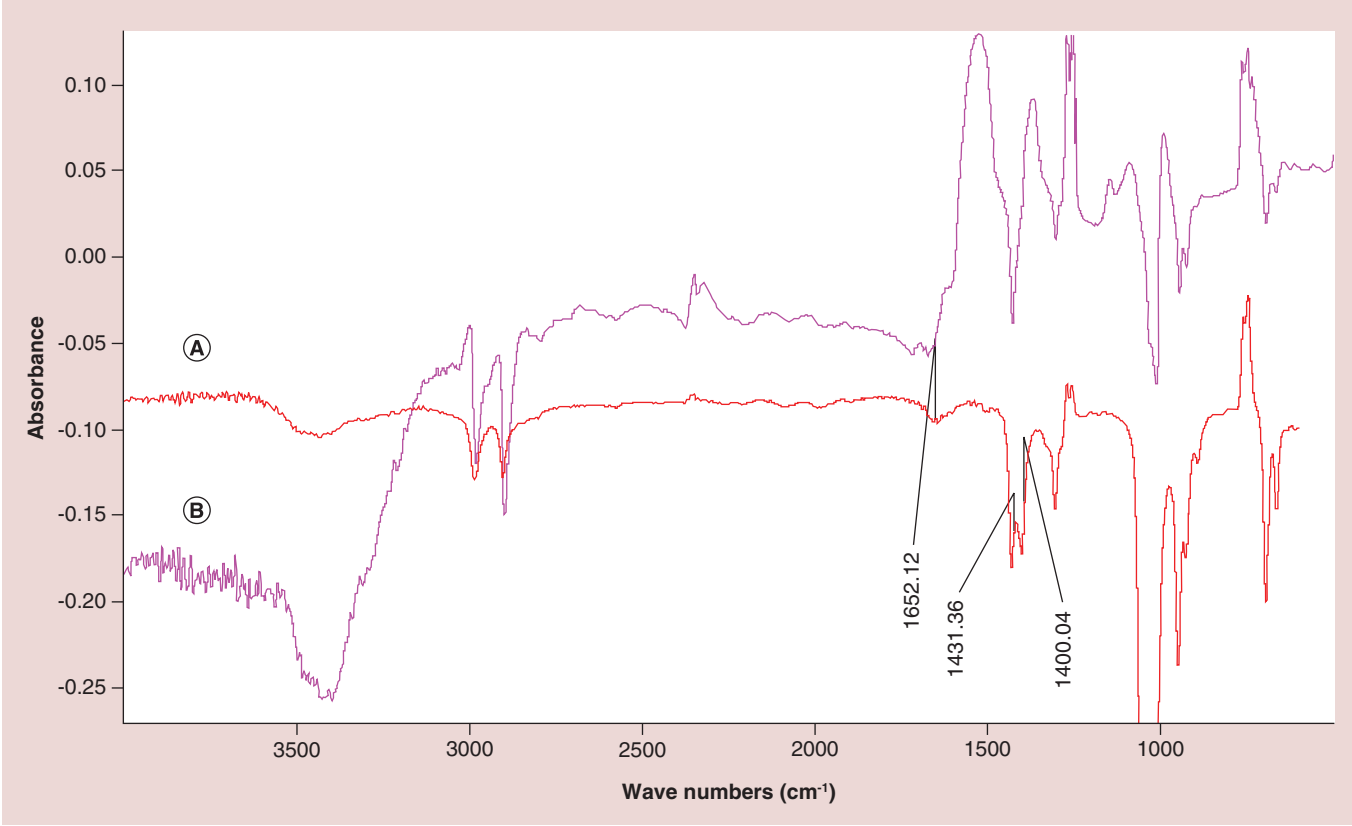

Figure 3. Characterization of the polymers by fourier transform infrared spectroscopy. Fourier transform IR spectra of thiolated chitosan **(A)** and mannose-modified thiolated chitosan **(B)**. The presence of amide carbonyl and hydroxyl bands in FTIR spectrum of the mannose-anchored thiolated polymer further confirms the association of the mannose sugar and the polymer backbone.

tion was induced by the addition of an aqueous solution of H_2O_2. Consequently, a decrease in the density of thiol groups within the nanocarriers was confirmed using the Ellman's reagent. Stability of the developed nanoformulations in terms of size, charge and PDI was evaluated under various storage temperatures (-20, 4 and 37°C) in a time-dependent manner. No notable changes in size, ζ-potential and PDI, were observed when the nanoformulations were kept for a period of 4 weeks at 4 and 37°C. However, statistically significant increases in average size and PDI (~2- and 1.5-fold, respectively) were observed for nanoformulations after 4 weeks at -20°C.

Drug release profiles

In this study, AmB release profiles of native drug powder, UC, TC and MTC nanocarriers were evaluated for 10 days at endosomal pH of 5.5 and physiological pH of 7.4. When assessing *in vitro* drug release of a hydrophobic drug, sink conditions were maintained. These conditions were maintained by inclusion of 1% (v/v) Tween in the phosphate buffer [17,19]. This allowed the total quantity of drug can be eluted from the nanocarriers and to reduce the adhesion of AmB onto the dialyzing membrane wall. The percentage of AmB released from the nanocarriers was evaluated in a time-dependent manner (Figure 5). The release patterns were biphasic (i.e., an initial burst release of 40% within 2 days followed by an extended sustained release for 10 days). Moreover, as observed from native drug powderm 100% drug was released in both settings within 1 h (data not shown). Therefore, release media provides a sufficient hydrophobic environment for complete dissolution of drug. The initial burst release of the drug might be the result of diffusion of loosely bound drug near the particle surface. During the second phase, both TC and MTC nanocarriers exhibited a slow sustained release of AmB for up to 10 days, compared with >80% of drug released from UC nanocarriers within 4 days, possibly due to poor stability of the UC polymeric network. It is also worth noting that both TC and MTC nanocarriers exhibited the lowest initial drug release as compared with UC.

Biocompatibility screening studies

The biocompatibility of the developed nanoformulation was evaluated in J774 cells using the MTT assay.

tosan–TGA conjugate is illustrated in Figure 1. Successful synthesis of the conjugate was confirmed by ^{1}H NMR and FTIR spectroscopy. The ^{1}H NMR spectrum of MCT is shown in Figure 2. Peaks in the region of 3.5–3.9 ppm and 4.5–5.1 ppm correspond to methylene protons (CH_2 group) of the mannose sugar. These were present in the final product spectrum but not in the starting material (Figure 2A & B, respectively). The FTIR spectra of the TC and mannose-modified TC are illustrated in Figure 3. A characteristic band at 3363 cm^{-1} corresponds to stretching vibrations of $–NH_2$ and –OH functional groups. The band at 2375 cm^{-1} corresponding to thiol groups was observed in the TC spectrum (Figure 3). For the mannose-modified TC, new peaks at 1652, 1431 cm^{-1} and 1400 cm^{-1} corresponds to amide bond formation and –OH stretching vibrations, an indication that the mannose sugar was incorporated on the polymer backbone.

AmB loaded UC, TC and MTC nanocarriers were manufactured by a blend of embedding and diffusion. The payload of AmB-loaded nanocarriers was from 21 to 72% (Table 1). Based on our prior experience, 0.54 µM TPP is required for cross-linking Chito and 0.60 µM for TC and MTC nanocarriers to stabilize the particles. The morphologies of the synthesized nanocarriers were rod-shaped (Figure 4). Nanoparticle surface chemistry and parameters influence nanoformulation stability and attachment onto biological surfaces. The average ζ-potentials of MTC (19 ± 3) and TC (21 ± 0.6) were found to be lower than that of UC (28 ± 4) ($p < 0.05$) nanocarriers. The decrease in the ζ-potential of MTC was the result of mannose immobilization onto the polymer backbone. Moreover, all the nanoparticles were found to have a moderate PDI and narrow size distribution as illustrated in Table 2. To further stabilize TC and MTC nanocarriers, inter- and intramolecular disulfide bond forma-

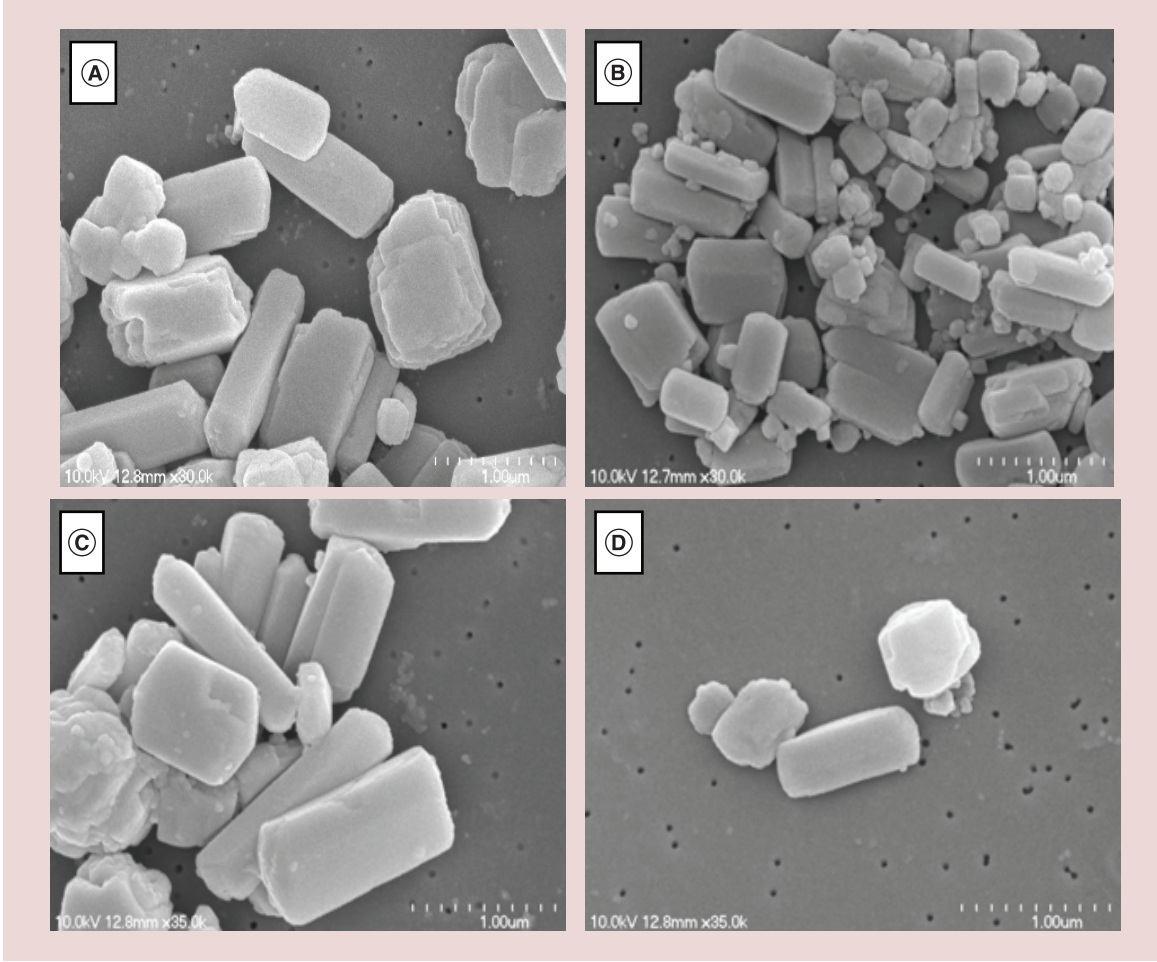

Figure 4. Nanoparticle morphologies. SEM images of unmodified chitosan **(A)**, thiolated chitosan **(B)** and mannose-anchored thiolated chitosan **(C)** nanocarriers before centrifugation and SEM image of mannose-anchored thiolated chitosan **(D)** after centrifugation.
SEM: Scanning electron microscopy.

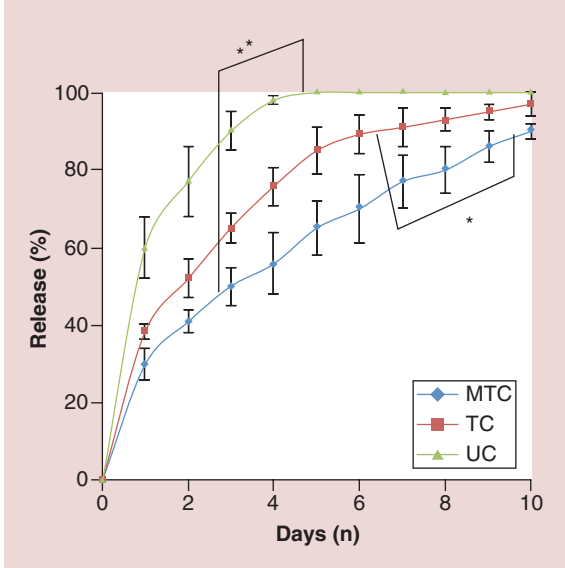

Figure 5. Release profile of developed nanoformulations. Dissolution studies were performed in phosphate buffer pH 7.2 at 37°C. Values are mean ± SD of three experiments. Statistically significant differences in the release profile of MTC were determined compared with TC and UC at significance levels of *p < 0.05; **p < 0.01.
MTC: Mannose-anchored thiolated chitosan; SD: Standard deviation; TC: Thiolated chitosan; UC: Unmodified chitosan.

J774 cells were incubated with various concentrations of AmB nanoformulations (0, 25, 50 and 75 µg/ml AmB). Differences were observed in the cytotoxicity profiles between TC and MTC, UC ($p \leq 0.05$) and native drug ($p \leq 0.05$). With MTC >90 ± 4.3% cell survival over 72 h was observed at the highest concentration tested (75 µg/ml AmB), while native drug solution reduced cell viability to 34.5 ± 5.6% (n = 3 ± SD) as shown in Figure 6. The values for the negative control Triton X-100 (2% v/v) and the positive-control medium without fetal calf serum/phenol red showed 0.40 ± 0.03% and 100.8 ± 4% viability, respectively.

Internalization of MTC AmB nanocarriers by macrophages

Cellular internalization of targeted (TC and MTC), nontargeted (UC), AmBisome and native drug after 12 h incubation was compared in sensitive and resistant *L.* donovani infected or uninfected control cells following drug nanoformulation treatments (100 µM). UC nanocarriers, AmBisome and native drug showed reduced uptake into infected cells with the resistant VL strain after 12-h incubation ($p \leq 0.05$) (Table 3). To determine whether MDR1 is involved in the efflux of AmB, pretreatment with verapamil, an inhibitor of MDR1 was tested. Here retention of AmB from UC, AmBisome and native drug solution in infected and uninfected macrophages was evaluated (Table 3). Pretreatment with verapamil demonstrated partial reversal of the efflux process, as the uptake of AmB was 2-, 2.5-, 1.2-fold higher from UC, AmBisome and native drug solution, respectively, for the resistant strain-infected macrophages. However, the uptake of the uninfected macrophages and sensitive strain-infected macrophages was not altered significantly by pretreatment with verapamil. These observations suggest that the lower intracellular AmB concentration in the resistant strain-infected macrophages compared with noninfected macrophages and sensitive strain-infected macrophages may be the result of upregulated drug efflux machinery. TC and MTC nanocarriers (100 µM) were rapidly internalized into the noninfected macrophages and drug concentrations of up to 12.9 ± 2.3 µg of AmB/10^6 cells and 28.6 ± 1.4 µg AmB/10^6 cells over 12 h, respectively. We observed the uptake of TC and MTC to be 4.2- and 9.6-fold higher, respectively, in resistant strain-infected macrophages compared with unmodified nonthiolated nanocarriers (Table 3). The results reported in this work therefore suggest that the thiolated surface-modified nanocarriers contribute to inhibition of AmB efflux in resistant strain-infected macrophages. MTC nanoparticles showed 71.5-, 26.0-, 4.4- and 2.2-fold increases in uptake by noninfected macrophages at 12 h compared with equimolar concentrations of TC ($p \leq 0.05$), UC ($p \leq 0.05$), AmBisome ($p \leq 0.05$) and native drug ($p \leq 0.001$), respectively, Table 3.

The amount of drug lost during the washing steps of cellular internalization was determined by HPLC analysis of the supernatants. It was observed that loss of drug in the washed volume was decreased with longer incubation time (data not shown). Interactions of the nanocarriers with the cell surface seem to be time dependent. Moreover, UC, AmBisome and native drug displayed higher drug loss in contrast to TC and MTC nanocarriers.

We also investigated the drug retention profile of the developed nanocarriers over 10 days (Figure 7). There were significant differences in the drug retention profile ($p \leq 0.05$) between AmBisome and native drug when cells were treated with equimolar drug concentrations. Specifically, 0.34 µg of AmB/10^6 cells was detected 2 days after treatment with AmBisome, compared with none for the native drug. UC nanocarriers were found to keep the drug inside the cells for 8 days. The TC and MTC nanocarriers retained and slowly released AmB over the 10-day period.

Antileishmanial activities

In this study, various AmB nanoformulations were synthesized and investigated against *L. donovani* amastigotes in a concentration-dependent manner (Figure 8).

Free AmB and AmBisome were used as controls. Drug-free nanocarriers (UC, TC and MTC) were used as additional controls. As shown in Figure 8A, AmB, AmBisome UC, TC and MTC nanocarriers at doses equivalent to 1.0 µg/ml AmB showed 48% ± 6%, 60% ± 11%, 76% ± 9%, 84% ± 7% and 96% ± 2% inhibition of parasites, respectively. The measured IC_{50} of AmB, AmBisome, UC, TC and MTC nanocarriers was found to be 0.256 ± 0.013 µg/ml, 0.208 ± 0.01 µg/ml, 0.164 ± 0.03 µg/ml, 0.096 ± 0.004 µg/ml and 0.019 ± 0.007 µg/ml, respectively. Macrophage targeting through mannose-anchored thiolated nanocarriers significantly improved the antileishmanial activity of AmB against intracellular parasites. Further evaluation of the potential application and future development of the synthesized nanoformulations as slow acting antileshmania therapies were conducted over a 10-day period. The native drug exhibited limited antimicrobial responses (data not shown). In contrast, MTC showed extended activity against *L. donovani*, suppressing parasite replication by 3.4-fold on the 10th day.

The *in vivo* therapeutic efficacy of MTC nanocarriers at a single dose of 1 mg AmB/kg was evaluated in *L. donovani*-infected mice and compared with native AmB. The observed findings were then validated with AmBisome. The results showed that MTC nanocarriers were considerably more effective (89% ± 7% inhibition) than AmB (17% ± 4% inhibition) ($p < 0.001$). Whereas TC, UC, AmBisome and nanocarriers alone had 63% ± 5%, 36% ± 2%, 19% ± 2.4% and 11% ± 1% reductions in parasites, respectively. Among all tested formulations, MTC demonstrated the greatest antileishmanial efficacy.

Discussion

For a spectrum of infectious diseases that include leishmaniasis, tuberculosis and HIV, macrophages serve as critical reservoirs and site of microbial replication for the intracellular microorganisms. Limited access of therapeutic agents to intracellular sites remains a major obstacle to effective anti-infectious disease therapy. In addition to reducing nonspecific drug toxicity, selective targeting of intramacrophage parasites with ligand-anchored nanocarrier delivery systems would facilitate pathogen clearance by ensuring that drug concentrations at these sites remain within the desired therapeutic range. In order to achieve this goal, mannose receptor-mediated endocytosis of drug nanocarriers by macrophages has become increasingly attractive. In the present study, MTC nanocarriers were synthesized, characterized and evaluated against intramacrophage amastigote parasites.

Chitosan-based nanocarriers are widely used for drug delivery applications owing to their efficient intracellular release of drug payloads and biocompatibility. Thiolated polymers such as TC [20] promote nanoparticle internalization owing to their unique properties. Mannose modification of the TC polymer was used to improve uptake of the drug carrying particles by macrophages where *Leishmania* amastigotes reside. Nanocarriers for macrophage delivery may offer numerous advantages over traditional delivery, including enhanced treatment rates, reduced off-target adverse effects, amplified drug stability and successful intracellular targeting. The MTC nanocarriers were manufactured and characterized by various analytical techniques, including FTIR, ^{1}H NMR and scanning electron microscopy. The results of mannose anchoring were consistent with the earlier described mannosylation of nanocarriers with amino groups of polymer [2]. UC, TC and MTC nanocarriers were formulated by homogenization followed by ionic gelation with TPP and generation of intra- and intermolecular disulfide bonds. Rod-shaped morphologies of the nanocarriers could be due to a par-

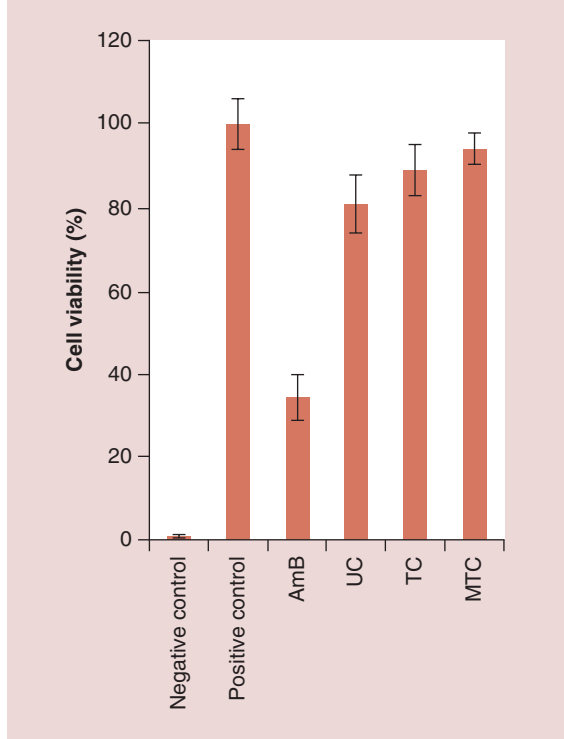

Figure 6. Biocompatibility of nanoformulations in J744A.1 cells after 72 h incubation. To retain equivalent concentrations, nanoformulations of MTC (0.93 µg/ml), TC (1 µg/ml) and UC (1.6 µg/ml) were dissolved to achieve concentrations of 75 µg/ml AmB in the culture medium. Results are expressed as mean ± SD of three replicate wells at significance levels of **$p < 0.01$; ***$p < 0.001$.
MTC: Mannose-anchored thiolated chitosan; SD: Standard deviation; TC: Thiolated chitosan; UC: Unmodified chitosan.

ticular characteristic of homogenized hydrophobic drug particles.

For *in vivo* applications, it is highly desirable to design a carrier that is stable and provides sustained release of therapeutic agents during systemic circulation. In the systemic circulation, the stability of the drug carrier is key to minimizing rapid elimination of the drug from the body. Hence, drug release was carried out at endosomal pH of 5.5 and physiological pH of 7.4 containing 1% (v/v) Tween-80. An initial burst release of drug (~ 40% within 2 days) was observed with TC and MTC nanocarriers followed by a slow-release phase, which continued for 10 days. In contrast, UC nanocarriers released 80% of drug within 4 days. A possible explanation for the observed sustained drug release from TC and MTC nanocarriers may be due to covalent cross-linking of disulfide bonds formed within the modified polymer matrix during the swelling process [21]. Moreover, all developed nanocarriers released >55% of drug at endosomal pH 5.5 (data not shown). This faster release at endosomal pH may be the result of increased solubility of AmB and the polymer under acidic conditions. The extent of oxidation of immobilized thiol groups via thiol (-SH)/disulfide (-S-S-) exchange reactions was found to be greater at physiological pH due to thiolate anion (RS^-) formation at high pH. Therefore, these findings support the use of modified chitosan nanoparticles for sustained and controlled release of drug payloads at intracellular infection sites.

Table 3. Comparison of uptake of amphotericin B from targeted (thiolated chitosan and mannose-anchored thiolated chitosan) nanocarriers, unmodified chitosan nanocarriers, AmBisome® and native drug in uninfected macrophages.

Formulations	Uptake studies (μg AmB/10^6 cells)			p-value
	Uninfected macrophages	Sensitive strains-infected macrophages	Resistant strains-infected macrophages	
AmB	0.4 ± 0.01	0.38 ± 0.02	0.04 ± 0.006	0.058^x 0.0002^y 0.0003^z
AmBisome	1.1 ± 0.07	1.2 ± 0.08	0.3 ± 0.05	0.061^x 0.007^y 0.0073^z
UC	6.5 ± 0.9	6.3 ± 0.7	2.9 ± 0.4	0.055^x 0.0004^y 0.0003^z
TC	12.9 ± 2.3	11.5 ± 1.1	12.3 ± 2.2	0.056^x 0.071^y 0.069^z
MTC	28.6 ± 1.4†***,‡**,§*,¶*	27.9 ± 1.6†***,‡**,§**,¶*	28.1 ± 1.7†***,‡**,§**,¶*	0.059^x 0.063^y 0.064^z
Pretreatment with verapamil				
AmB	0.39 ± 0.02	0.36 ± 0.03	0.084 ± 0.01	0.061^x 0.003^y 0.004^z
AmBisome	1.2 ± 0.06	1.3 ± 0.09	0.76 ± 0.05	0.079^x 0.009^y 0.008^z
UC	6.6 ± 0.8	6.2 ± 0.5	3.5 ± 0.9	0.062^x 0.004^y 0.003^z

Both resistant and sensitive *Leishmania donovani* were used to infect macrophages. Data are expressed as three replicates in all tests, and the data are expressed as mean ± SD of three independent experiments. Statistically significant differences of MTC were determined in relation to AmB solution (†), AmBisome (‡), UC (§) and TC (¶) at significance levels of *p < 0.05; **p < 0.01; ***p < 0.001. x = probability value between uninfected macrophage group and sensitive strain-infected macrophage group; y = probability value between uninfected macrophage group and resistant strain-infected macrophage group; z = probability value between sensitive strain-infected macrophage group and resistant strain-infected macrophage group.
AmB: Amphotericin B; MTC: Mannose-anchored thiolated chitosan; SD: Standard deviation; TC: Thiolated chitosan; UC: Unmodified chitosan.

The biocompatibility induced by nanoformulations and native drug was assessed at various concentration (0, 25, 50 and 75 µg/ml AmB) in J774 cells by using the MTT cell proliferation assay. The rank order of biocompatibility at highest concentration was MTC>TC>UC> AmBisome > AmB. Higher biocompatibility of thiolated nanoformulations (TC and MTC) could be due to the surface modification, where less ionizable-free amino groups are available in TC and MTC as compared with UC. Moreover, surface-modified nanocarriers resulted in an enormously significant decline ($p \leq 0.05$) in the cytotoxicity of AmB. Our findings are similar to those previously reported where surface-modified nanocarriers were used to deliver AmB [2]. The toxicity of AmB has been associated with the formation of drug aggregates [2]. It has been demonstrated that the nonaggregated form of AmB is biocompatible toward mammalian cells but causes porosity of parasitic cells. The aggregated form of AmB forms pores in both mammalian and parasitic cell membranes. The decline in cytotoxicity of AmB encapsulated into surface-modified nanocarriers could be linked, in measure, to the slow release of nonaggregated drug.

Since macrophages serve as reservoirs for *Leishmania* amastigotes, receptor-mediated endocytosis of drug nanocarriers is essential in ensuring the delivery of high intracellular drug concentrations required to clear the parasite. We therefore sought to design and study MTC nanocarriers for cellular internalization of antileishmanial agents. The cellular internalization of nanoformulations and native drug was compared in sensitive and resistant *L. donovani*-infected or -uninfected control cells. Overexpression of ABC transporters especially MDR1 is well known to be an important mechanism of drug efflux for *L. donovani*-resistant strains [18]. Hence, lower cellular internalization of UC nanocarriers, AmBisome and native drug into cells infected with the resistant VL strain could be due to upregulated drug efflux machinery. In contrast, no significant difference in cellular internalization profile of TC and MTC was seen in sensitive and resistant *L.* donovani-infected or -uninfected control cells. Efflux pump inhibitory capability of thiolated polymers has been shown in mammalian cells [11]. Dünnhaupt *et al.* demonstrated that thiolated polymers inhibit the efflux pump by blocking the efflux pump drug-binding sites [22]. Accordingly, TC and MTC may be also responsible for the inhibition of drug efflux machinery in the resistant VL strain.

Thiol-reactive groups have also been shown to promote binding and cellular internalization of nanomaterials [13,23,24]. A recent study on thiolated surface-stabilized superparamagnetic iron oxide nanoparticles

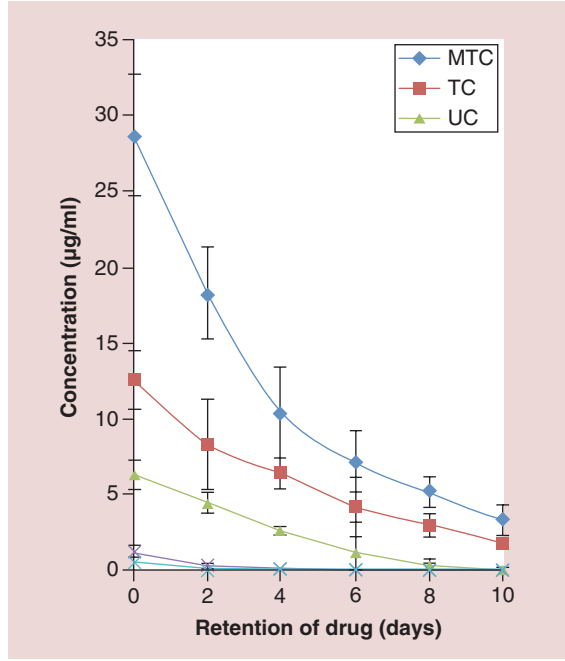

Figure 7. Intracellular retention of MTC, TC, UC nanocarriers, AmBisome® and native drug in macrophages determined over 10 days. Retention of drug was observed along with sustained release. Data are shown as mean ± SD of three replicate wells. ***p < 0.001 (comparison of MTC versus AmB and AmBisome); **p < 0.01 (comparison of MTC versus TC and UC nanocarriers).
AmB: Amphotericin B; MTC: Mannose-anchored thiolated chitosan; SD: Standard deviation; TC: Thiolated chitosan; UC: Unmodified chitosan.

demonstrated efficient internalization of thiol surface-modified nanoparticles by stem cells. It was found that decorating the magnetic particles with thiol moieties resulted in a 17-fold increase in uptake by progenitor cells when compared with nonthiolated superparamagnetic iron oxide nanoparticles [20]. These findings provide additional support to the concept that the presence of thiol groups on the surface of the particles could enhance cellular internalization. Accordingly, a 1.98-fold increase in uptake of TC by noninfected macrophages was observed over equivalent concentrations of UC nanocarriers. Further improvement in AmB cellular uptake was seen when MTC was used as the drug carrier. The increase in uptake for the mannose-anchored MTC over the TC may be due to the mannose receptor-mediated endocytosis of the drug particles. The macrophage-targeted MTC drug delivery system therefore represents a promising approach to *Leishmania* eradication that would allow for delivery of effective drug concentrations at sites of amastigote replication. Efficient internalization of MTC into macrophages may proceed by either specific or nonspecific mechanisms that include: access and initial interaction

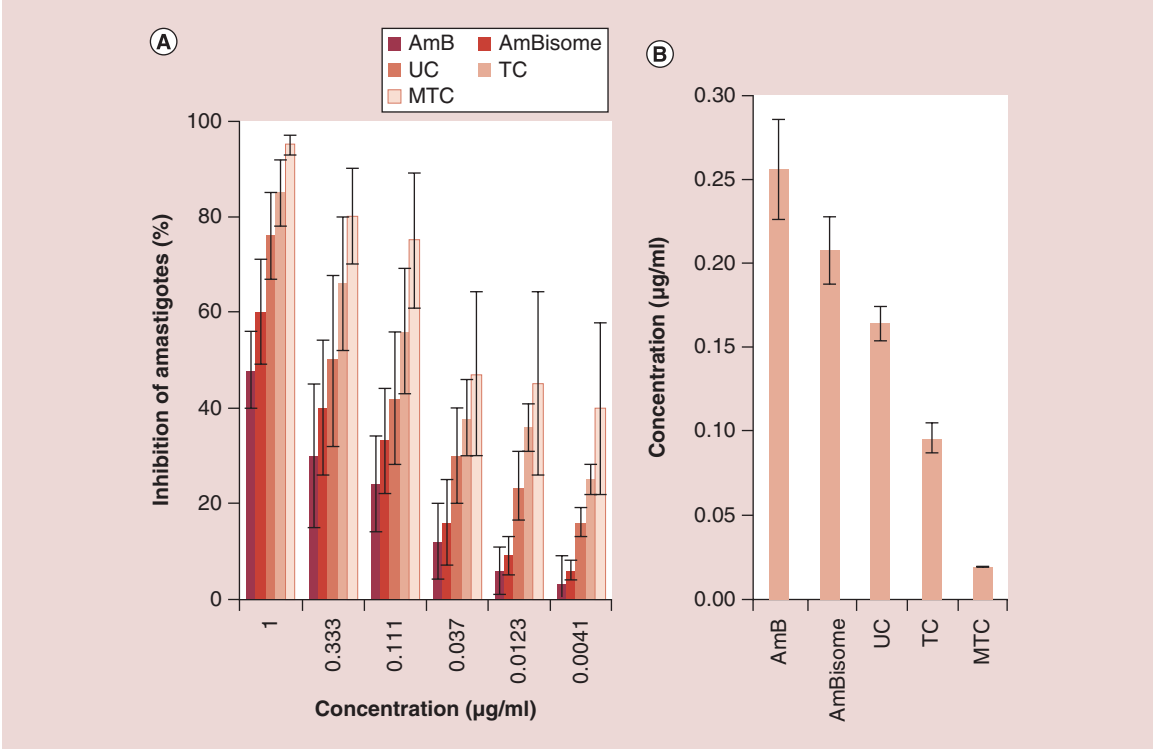

Figure 8. Pharmacological evaluation of antileishmanial activities. Percent inhibition of *Leishmania donovani* amastigotes by escalating concentration (ug/ml) of AmB, AmBisome, UC, TC and MTC **(A)**. For **(B)** the concentration (ug/ml) required to achieve an *in vitro* (IC_{50}) activity against *L. donovani* amastigotes. All experiments were performed with human MDM infected with the parasite for a 12 h incubation **(B)**. Concentration of the polymer used in nanoformulation was biocompatible to the target macrophage. Data expressed as mean ± SD for a representative of one or three performed experiments.
AmB: Amphotericin B; MDM: Monocyte-derived macrophages; MTC: Mannose-anchored thiolated chitosan; SD: Standard deviation; UC: Unmodified chitosan.

of nanocarriers with the surface membrane of macrophages; interaction of reactive thiol moieties on the surface of MTC with the macrophage membrane; recognition of MTC by mannose phagocytic machinery expressed on the macrophage surface; and configurational changes in the cell membrane structure (projection or invagination), vacuolization and internalization of the drug particles. Therefore, increased intracellular drug concentrations and prolonged retention exhibited by MTC are all important aspects in the development of nanoformulations that would target and eradicate intracellular infections.

Superior cellular retention profiles of the UC, TC and MTC nanocarriers as compared with AmBisome and native drug could be due to cationic chitosan polymeric backbone. Chitosan-based nanocarriers are known to escape from the endosomes thereby able to escape lysosomal degradation and deliver the drug payload to the target site [25]. This phenomenon that is common to cationic polymers is referred to a proton sponge effect [26]. In addition, the extended sustained and slow release of drug for TC and MTC nanocarriers might be the result of interactions between thiol moieties of the nanocarriers and the disulfide bonds of the lysosomal enzyme via thiol/disulfide exchange reaction (SH → -S-S-; -S-S- → -SH). This prolonged retention profile would allow for a reduced dosing frequency.

Leishmania parasites have two main life-cycle phases: the extracellular motile promastigotes phase, found in the phlebotomine sandflies vector and the intracellular immotile amastigotes phase that thrives in the mammalian host. Amastigotes proliferate in the macrophage parasitophorous vacuoles, phagolysosome-like compartments with hydrolytic and acidic surroundings. Parasitophorous amastigotes lead to destruction of the host cell but manage to escape into the systemic circulation where they are adept at infecting new phagocytic cells and responsible for the pathogenesis of leishmaniasis. Targeted drug delivery to parasite reservoirs such as macrophages is anticipated to increase the therapeutic efficacy and diminish off-target drug toxicity. For antileishmanial activity against parasitophorous *L. donovani* amastigotes-infected macrophages, MTC again provided maximum inhibition of the parasite. Low drug concentrations of the MTC formulation were able to inhibit intracellular

parasite replication when compared with the clinically used AmBisome formulation ($p < 0.05$). The IC_{50} of MTC was 13.0-, 10.6-, 8.4- and 4.9-fold lower than that of AmB ($p < 0.05$), AmBisome ($p < 0.05$), Chito ($p < 0.05$) and CT ($p < 0.05$), respectively. The observed improvement in antileishmanial activity of the MTC AmB nanocarrier could be the result of localized delivery of the therapeutic agent at intracellular sites that harbor the parasites.

Oral MTC nanoformulation was highly efficacious in infected rodents. These results support our laboratory findings of enhanced antimicrobial activities of the nanoformulations. The efficacy of the MTC nanoformulations was significantly greater than that of the AmB solution. This improved efficacy may be associated with an improved cellular internalization of the drug formulations with a favored accumulation in the reticuloendothelial system.

We found drug-free MTC control nanoformulations to exhibit antileishmanial activity. Mannosylated nanocarriers have been shown to generate signals following engulfment or interaction with phagocytic cells, in particular macrophages, which leads to macrophage stimulation and upregulation of cytokines [17]. Inducible nitric oxide synthase and consecutive generation of nitric oxide has been shown to exhibit antimicrobial effect [27]. The chitosan polymer has been reported to trigger a proinflammatory response such as nitric oxide production that stimulates macrophages and this could lead to parasiticidal activity [17,27]. Hence, antileishmanial activity of drug-free nanocarriers based on chitosan polymeric backbone could be due to nitric oxide production. Therefore, higher drug uptake and successful killing of *L. donovani* parasites by the MTC formulation are expected to attain the preferred therapeutic outcome at a lower dose.

Conclusion

Long acting macrophage-targeted MTC nanocarriers loaded with AmB were successfully synthesized and evaluated for cellular uptake and antileishmanial responses. The mannosylated nanocarriers displayed enhanced uptake of the encapsulated AmB by macrophages when compared with uptake of native drug or nontargeted particles. Interestingly, the mannosylated system was found to retain the drug inside the macrophages for up to 10 days. The MTC nanocarriers were also found to be highly effective at inhibiting the growth of intracellular amastigotes in infected macrophages when compared with native drug. These encouraging *in vitro* data provide proof-of-concept that macrophage-directed TC nanocarriers hold promise as potential therapies for parasitic and other intracellular infections.

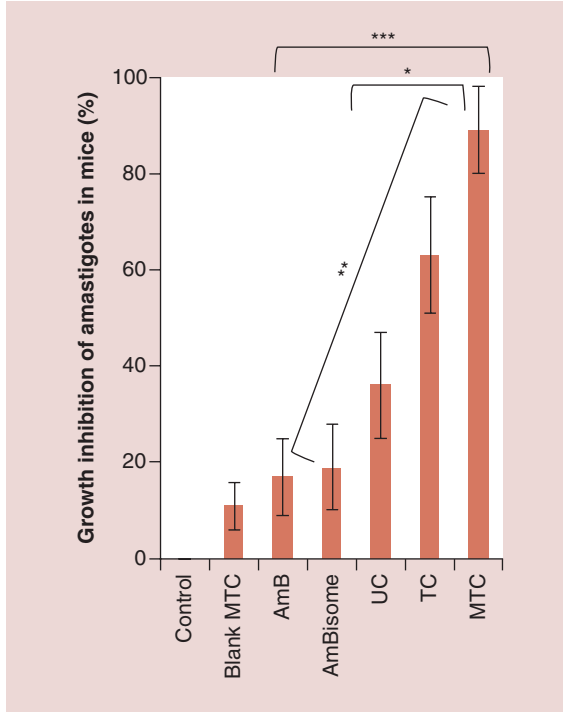

Figure 9. *In vivo* therapeutic efficacy of oral MTC, TC, UC, AmB and blank MTC nanocarriers (AmB free) in BALB/c mice infected with *Leishmania donovani* at an oral dose of 1 mg of AmB/kg body weight.
AmBisome® was injected intravenously, as an additional control, into mice on the 4th week of infection. Data are expressed as median values ± SD and significant differences were determined by Kruskal–Wallis test, followed by Dunn's posthoc test with significance levels *$p < 0.05$; **$p < 0.01$; ***$p < 0.001$.
AmB: Amphotericin B; MTC: Mannose-anchored thiolated chitosan; SD: Standard deviation; TC: Thiolated chitosan; UC: Unmodified chitosan.

Future perspective

AmB for VL is currently administered by parenteral route because of poor oral bioavailability. But high cost and associated nephrotoxicity have restricted parenteral administration of AmB. Therefore, development of an oral formulation of AmB for VL will help overcome these limitations. The synthesized mannosylated and TC delivery system with permeation enhancing, *in situ* gelling, sustained release, mucoadhesion and P-glycoprotein inhibitory properties has the potential to improve oral bioavailability and efficacy of AmB.

Acknowledgements

The authors thank KP Chang and S Rana for technical assistance and active research discussions. The authors also acknowledge the assistance of the University of Nebraska Lincoln Electron Microscopy Core Facility.

Financial & competing interests disclosure

This work was supported by the UNESCO-L'Oréal International Fellowship for Young Women in Life Sciences and NIH grants P01 DA028555, R01 NS36126, P01 NS31492, 2R01 NS034239, P01 MH64570, P01 NS43985, P30 MH062261 and R01 AG043540. The authors have no other relevant affiliations or financial involvement with any organization or entity with a financial interest in or financial conflict with the subject matter or materials discussed in the manuscript apart from those disclosed.

No writing assistance was utilized in the production of this manuscript.

Ethical conduct of research

The authors state that they have obtained appropriate institutional review board approval or have followed the principles outlined in the Declaration of Helsinki for all human or animal experimental investigations. In addition, for investigations involving human subjects, informed consent has been obtained from the participants involved.

Executive summary

- Mannose-anchored thiolated chitosan (MTC) nanocarriers were designed and evaluated against intramacrophage amastigote parasites.
- Surface-modified nanocarriers resulted in an enormously significant decline in the cytotoxicity of amphotericin B.
- Thiolated chitosan and MTC nanocarriers were rapidly internalized into the macrophages and contributed to inhibition of amphotericin B efflux in resistant strain-infected macrophages.
- At lower concentrations, the MTC formulation were able to inhibit intracellular parasite replication as compared with the AmBisome®.
- Finally, MTC nanocarriers emerge to be a promising nanomedical tool for the treatment of leishmaniasis.

References

Papers of special note have been highlighted as: • of interest; •• of considerable interest

1 Yasinzai M, Khan M, Nadhman A, Shahnaz G. Drug resistance in leishmaniasis: current drug-delivery systems and future perspectives. *Future Med. Chem.* 5(15), 1877–1888 (2013).

• **Expert opinion on therapeutic strategies for visceral leishmaniasis.**

2 Jain K, Verma AK, Mishra PR, Jain NK. Surface-engineered dendrimeric nanoconjugates for macrophage-targeted delivery of amphotericin B: formulation development and *in vitro* and *in vivo* evaluation. *Antimicrob. Agents Chemother.* 59(5), 2479–2487 (2015).

3 Asthana S, Gupta PK, Jaiswal AK, Dube A, Chourasia MK. Overexpressed macrophage mannose receptor targeted nanocapsules-mediated cargo delivery approach for eradication of resident parasite: *in vitro* and *in vivo* studies. *Pharm. Res.* 32(8), 2663–2677 (2015).

•• **Describes macrophage mannose receptor-targeted antileishmanial therapy.**

4 Jain K, Verma AK, Mishra PR, Jain NK. Characterization and evaluation of amphotericin B loaded MDP conjugated poly(propylene imine) dendrimers. *Nanomedicine* 11(3), 705–713 (2015).

5 Chaubey P, Mishra B. Mannose-conjugated chitosan nanoparticles loaded with rifampicin for the treatment of visceral leishmaniasis. *Carbohydr. Polym.* 101, 1101–1108 (2014).

6 Dutta T, Agashe HB, Garg M, Balakrishnan P, Kabra M, Jain NK. Poly (propyleneimine) dendrimer based nanocontainers for targeting of efavirenz to human monocytes/macrophages *in vitro*. *J. Drug Target.* 15(1), 89–98 (2007).

7 Sarkar K, Das PK. Protective effect of neoglycoprotein-conjugated muramyl dipeptide against *Leishmania donovani* infection: the role of cytokines. *J. Immunol.* 158(11), 5357–5365 (1997).

8 Jain NK, Mishra V, Mehra NK. Targeted drug delivery to macrophages. *Expert Opin. Drug Deliv.* 10(3), 353–367 (2013).

9 Yeeprae W, Kawakami S, Higuchi Y, Yamashita F, Hashida M. Biodistribution characteristics of mannosylated and fucosylated O/W emulsions in mice. *J. Drug Target.* 13(8–9), 479–487 (2005).

• **Describes the synthesis and characterization of thiolated polymers.**

10 Kast CE, Bernkop-Schnurch A. Thiolated polymers–thiomers: development and *in vitro* evaluation of chitosan-thioglycolic acid conjugates. *Biomaterials* 22(17), 2345–2352 (2001).

•• **Describes the synthesis of nanoparticles followed by *in vitro* and *in vivo* studies.**

11 Palmberger TF, Hombach J, Bernkop-Schnurch A. Thiolated chitosan: development and *in vitro* evaluation of an oral delivery system for acyclovir. *Int. J. Pharm.* 348(1–2), 54–60 (2008).

12 Shahnaz G, Vetter A, Barthelmes J *et al.* Thiolated chitosan nanoparticles for the nasal administration of leuprolide: bioavailability and pharmacokinetic characterization. *Int. J. Pharm.* 428(1–2), 164–170 (2012).

13 Vetter A, Reinisch A, Strunk D *et al.* Thiolated polyacrylic acid-modified iron oxide nanoparticles for *in vitro* labeling and MRI of stem cells. *J. Drug Target.* 19(7), 562–572 (2011).

14 Veerareddy PR, Vobalaboina V, Ali N. Antileishmanial activity, pharmacokinetics and tissue distribution studies of mannose-grafted amphotericin B lipid nanospheres. *J. Drug Target.* 17(2), 140–147 (2009).

15 Yalpani M, Laurance DH. Some chemical and analytical aspects of polysaccharide modifications 3. Formation of branch-chain, soluble chitosan derivatives. *Macromolecules* 17, 272–281 (1984).

16 Javed I, Hussain SZ, Ullah I *et al.* Synthesis, characterization and evaluation of lecithin-based nanocarriers for the enhanced pharmacological and oral pharmacokinetic profile of amphotericin B. *J. Mater. Chem. B* 3(42), 8359–8365 (2015).

17 Asthana S, Jaiswal AK, Gupta PK, Pawar VK, Dube A, Chourasia MK. Immunoadjuvant chemotherapy of visceral leishmaniasis in hamsters using amphotericin B-encapsulated nanoemulsion template-based chitosan nanocapsules. *Antimicrob. Agents Chemother.* 57(4), 1714–1722 (2013).

18 Purkait B, Kumar A, Nandi N *et al.* Mechanism of amphotericin B resistance in clinical isolates of *Leishmania donovani*. *Antimicrob. Agents Chemother.* 56(2), 1031–1041 (2012).

19 Zhou W, Wang Y, Jian J, Song S. Self-aggregated nanoparticles based on amphiphilic poly(lactic acid)-grafted-chitosan copolymer for ocular delivery of amphotericin B. *Int. J. Nanomedicine* 8, 3715–3728 (2013).

20 Shahnaz G, Kremser C, Reinisch A *et al.* Efficient MRI labeling of endothelial progenitor cells: design of thiolated surface stabilized superparamagnetic iron oxide nanoparticles. *Eur. J. Pharm. Biopharm.* 85(3 Pt A), 346–355 (2013).

21 Shahnaz G, Perera G, Sakloetsakun D, Rahmat D, Bernkop-Schnurch A. Synthesis, characterization, mucoadhesion and biocompatibility of thiolated carboxymethyl dextran-cysteine conjugate. *J. Control. Release* 144(1), 32–38 (2010).

•• **Comprehensive study on thiomers as efflux pump inhibitors.**

22 Dunnhaupt S, Barthelmes J, Rahmat D *et al.* S-protected thiolated chitosan for oral delivery of hydrophilic macromolecules: evaluation of permeation enhancing and efflux pump inhibitory properties. *Mol. Pharm.* 9(5), 1331–1341 (2012).

•• **Explains the mechanism for cellular internalization of surface thiol groups.**

23 Aubry S, Burlina F, Dupont E *et al.* Cell-surface thiols affect cell entry of disulfide-conjugated peptides. *FASEB J.* 23(9), 2956–2967 (2009).

24 Rahmat D, Khan MI, Shahnaz G, Sakloetsakun D, Perera G, Bernkop-Schnurch A. Synergistic effects of conjugating cell penetrating peptides and thiomers on non-viral transfection efficiency. *Biomaterials* 33(7), 2321–2326 (2012).

25 Agirre M, Zarate J, Ojeda E, Puras G, Desbrieres J, Pedraz JL. Low molecular weight chitosan (LMWC)-based polyplexes for pDNA delivery: from bench to bedside. *Polymers (Basel, Switz.)* 6(6), 1727–1755, 1729 (2014).

26 Malatesta M, Grecchi S, Chiesa E, Cisterna B, Costanzo M, Zancanaro C. Internalized chitosan nanoparticles persist for long time in cultured cells. *Eur. J. Histochem.* 59(1), 2492 (2015).

27 Gupta PK, Jaiswal AK, Asthana S *et al.* Self assembled ionically sodium alginate cross-linked amphotericin B encapsulated glycol chitosan stearate nanoparticles: applicability in better chemotherapy and non-toxic delivery in visceral leishmaniasis. *Pharm. Res.* 32(5), 1727–1740 (2015).